VIDYA REPORT NO. 161
September 30, 1964

INTERFERENCE BETWEEN A HULL AND A STERN-MOUNTED DUCTED PROPELLER

by
Anthony R. Kriebel

Prepared under
Contract No. Nonr-4278(00)
Vidya Project No. 9066

This research was sponsored by the Bureau of Ships Fundamental Hydromechanics Research Program, S-R009 01 01, administered by the David Taylor Model Basin.

VIDYA
RESEARCH DEVELOPMENT
1450 PAGE MILL ROAD, PALO ALTO, CALIFORNIA
A DIVISION OF Itek CORPORATION

VIDYA COPY NO. 207

VIDYA REPORT NO. 161

September 30, 1964

INTERFERENCE BETWEEN A HULL AND A STERN-MOUNTED DUCTED PROPELLER

by

Anthony R. Kriebel

Prepared under
Contract No. Nonr-4278(00)
Vidya Project No. 9066

This research was sponsored by the Bureau of Ships Fundamental Hydromechanics Research Program, S-R009 01 01, administered by the David Taylor Model Basin.

VIDYA

A DIVISION OF Itek CORPORATION

1450 PAGE MILL ROAD • PALO ALTO, CALIFORNIA
TEL: DAVENPORT 1-2455 TWX: 415 492-9270

SUMMARY

The hydrodynamic interference between an underwater hull and a stern-mounted ducted propeller is predicted by theoretical analysis. The analysis assumes axially symmetric potential flow, and the hull wake vorticity is concentrated into multiple vortex cylinders extending downstream from the boattail. The interference forces are predicted versus the following geometric parameters with the hull shape held fixed to represent TMB Model 4620: duct chord-to-diameter ratio, duct size, duct axial spacing from hull, axial location of propeller within duct, duct camberline shape, and number of vortex cylinders used to represent hull wake. Also, the effect of duct profile thickness upon the analytical results is estimated and shown to be small.

The computed results show that cylindrical ducts are unsuitable for propulsion of the assumed hull shape because, at cruising speed, they are ineffective in reducing the propeller thrust, they have large leading-edge suction, and they produce large hull interference. However, when duct camber is added, the results also show that if all of the other geometric parameters are specified, a duct camberline can be designed so that the duct carries more thrust than the propeller without any leading-edge suction or hull interference.

TABLE OF CONTENTS

LIST OF TABLES

LIST OF FIGURES

LIST OF SYMBOLS

A	area of duct exit plane, πR^2
A_m	maximum cross-sectional area of hull, πR_m^2
A_n, A_n^*	Fourier coefficients for velocity induced by hull wake, Equation (14)
A_p	area of actuator disk, πR_p^2
B_n	Fourier coefficients for radial velocity induced by actuator disk, Equation (15)
C	drag coefficient for hull, or thrust coefficient for duct or propeller, based on duct exit area A and free-stream dynamic head q
C_n	Glauert coefficients for velocity induced by duct-bound vorticity, Equation (16)
C'	hull drag coefficient based on hull area A_m and q
c	chord length of duct
D	diameter of duct exit plane, $2R$
E,K	complete elliptic integrals of second and first kind, respectively
F	drag force
F_n	Fourier coefficients for velocity induced by hull, Equation (12)
f	dimensionless strength of a vortex cylinder in the hull wake, γ_W/V
k	argument for elliptic integrals, E,K, Equations (B.4) and (B.5)
L	length of hull
L_B	length of line sink, used to represent hull, Figure 1
L_Q	distance between point source and line sink used to represent hull, Figure 1
L_W	distance between leading edge of a hull wake cylinder and aft end of hull, Figure 1
$P_{k\ell}$	coefficients for velocity induced by duct-bound vorticity, Equation (17), Table II, Reference 5
Δp	actuator disk loading or pressure jump

Q	strengths of point source and line sink used to represent hull, Figure 1
q	dynamic head of free stream, $(1/2)\rho V^2$
q_D	ring source for duct profile thickness, Equation (D.1)
q_n	point source along hull boattail, Equation (B.6)
R	radius of duct exit plane
R_m	maximum hull radius
R_P	propeller radius when it is located within a cambered duct, equal to the duct radius at the propeller station
R_W	radius of a hull wake cylinder
$R_{o,1,2,3}$	Fourier coefficients for cambered duct, Equation (38)
r	radius from axis of symmetry, Figure 1
r_b	local radius of hull boattail, Figure 1
r_s	local radius of cambered duct, Sketch C, page 20
S	distance to duct inlet measured downstream from aft end of hull, Figure 1
T	thrust force
t	duct profile thickness
u	induced axial velocity component
V	free-stream velocity
V_j	jet velocity in slipstream of isolated ducted propeller, $V + \gamma$
v	induced radial velocity component
x, x_B, x_Q, x_s, x_W	axial distances defined in Figure 1
Z	parameter for propeller thrust coefficient, Equation (31), Table III
z	number of vortex cylinders used to represent hull wake
Γ	duct-bound circulation, Equation (B.1)
γ	strength of vortex cylinder shed by actuator disk, Figure 1
γ_D	strength of duct-bound vorticity, Figure 1
γ_W	strength of a vortex cylinder in hull wake, Figure 1

ϵ_n, ϵ_n^*	coefficients defined by Equations (41) and (45), respectively
θ	angular duct coordinate, arc cos $(-2x_s/c)$, Figure 1
ρ	density of free stream

Subscripts

B	hull boattail
D	duct
DP	ducted propeller
D(H)	duct thrust caused by hull
D(P)	duct thrust caused by propeller (represented as an actuator disk)
D(W)	duct thrust caused by hull wake
D_s	duct thrust due to leading-edge suction, Equation (19)
D_t	total duct thrust, Equation (48)
H	isolated hull
H(D)	hull drag caused by duct
H(P)	hull drag caused by propeller (represented as an actuator disk)
P	propeller (represented as an actuator disk)
Q	point source used to represent hull
q	point source along hull boattail
T	duct thickness
W	hull wake
Γ	duct-bound circulation, Sketch B.1
γ	propeller vorticity
γ_D	duct-bound vorticity
γ_W	vortex cylinders in the hull wake

Superscript

$( )'$	length $( )$ divided by duct radius R

BLANK PAGE

INTERFERENCE BETWEEN A HULL AND A STERN-MOUNTED DUCTED PROPELLER

1. INTRODUCTION

A theoretical investigation is being conducted of the interference between an underwater hull and a stern-mounted ducted propeller. The work is being supported under the Bureau of Ships Fundamental Hydromechanics Research Program, administered by the David Taylor Model Basin. This report presents the results of the first year's investigation of this problem.

The present analysis appears to be the first theoretical treatment of a hull combined with a ducted propeller, although similar analyses have been carried out for unducted propellers (e.g., Ref. 1). One of the possible benefits of the addition of a duct to a propeller is in the reduction of noise. For a given total thrust, a maximum duct thrust and minimum propeller thrust may reduce the radiated sound which is generated both by the rotating pressure field and hull-induced vibrations. In this study, the net forces on the hull, duct, and propeller are determined for various assumed configurations of the ducted propeller. The objective of the program is to determine the conditions under which much of the required thrust can be transferred from the propeller to the duct without causing large hull-duct interference effects or unreasonable design constraints on the ducted propeller.

2. METHOD OF APPROACH

The present study is restricted to steady axially symmetric flow with no net force on the combined hull and ducted propeller. The forces involved are the hull drag in the presence of the ducted propeller, the duct thrust caused by the propeller and affected by the hull with its wake, and the thrust on the propeller represented as an actuator disk situated in the hull wake. The condition of no flow through the hull surface is satisfied only approximately by an iterative procedure. The method of concentrated singularities is employed with the assumed singularity distribution consisting of four components shown in Figure 1:

(1) A source-sink distribution along the hull centerline to represent the hull.

(2) Multiple vortex cylinders trailing from the hull boattail to represent the hull wake.

(3) A single vortex cylinder extending downstream from the trailing edge of the ducted propeller to represent its slipstream.

(4) A distribution of elementary vortex rings bound to the duct such that there is no flow through its surface or across its trailing edge.

The assumptions and iterative procedure for evaluating the foregoing singularity distribution will be described in the next section. The hull shape was chosen to approximate TMB Model 4620 as shown in Figure 2(b). The initial computations are restricted to thin, cylindrical ducts with chord-to-diameter ratio of 1/2. The effects of duct camber and increased chord are incorporated into the analysis subsequently. The effect of duct thickness is not included in the main analysis because the investigation in Appendix D indicates that the effect is small.

2.1 Analytical Assumptions

The first step in the analysis is to specify the source-sink distribution used to represent the hull and the placement of the vorticity distributions which are used to represent the hull wake, the duct, and the propeller. This process will be described next for each of the singularity components.

The Hull with Its Wake

Representation of two different isolated hulls in potential flow by a point source followed by a line sink of constant strength is shown in Figure 2. The theory is described in Appendix A. This simple analytical approximation is good for the entire torpedo hull. Only the submarine hull will be used in the following analysis, however. For this hull the analytical representation is good except near the ends. The shape of the hull nose has almost no effect upon the present analysis since the flow field is calculated only near the ducted propeller. However, rounding off the aft 5 percent of the hull length (Fig. 2(b)) may have an appreciable effect upon the analytical results. Nevertheless, the extreme simplicity of the foregoing representation of the hull seems to justify the approximation, since the aft end of the hull is deeply submerged within the hull boundary layer which is also represented only approximately near the end of the hull by the assumed vortex cylinders. The drag coefficient of the hull alone is taken to be slightly smaller than the value measured for the TMB hull Model 4620 of Reference 1.

If the vorticity which is shed from the hull into its boundary layer and wake were concentrated into a finite number of vortex sheets, these sheets

would be surfaces of revolution as indicated in Sketch A, and the strength of each would vary over its length.

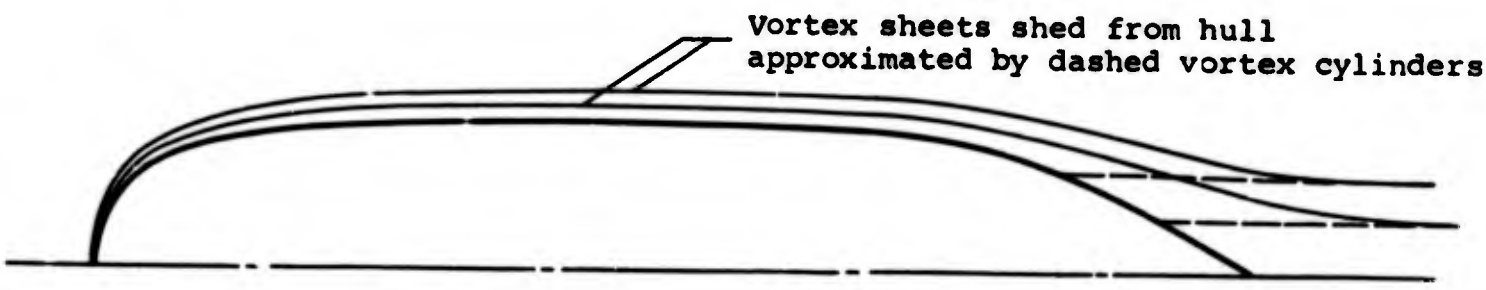

Sketch A.- Distribution of vorticity shed from hull.

The boundary layer over most of the hull is so thin that its effect on the external flow can be neglected. However, the boundary layer near the boattail and the hull wake may have a significant effect upon the flow over the duct. An attempt is made to account for the effect in the present analysis by approximating the distribution of vorticity shed from the hull by a finite number of vortex cylinders as shown in Sketch A. These cylinders extend downstream from the hull boattail, and each one is of constant strength. The sizes and strengths of the cylinders are selected in Section 3.1 to give a wake velocity distribution far downstream which approximates that measured one hull diameter aft of TMB Model 4620.

The hull wake cylinders are used only to account for the hull drag and the effect of the hull wake upon the flow over the duct and through the propeller. The flow induced by the cylinders through the hull surface is neglected. The cylinders could be extended upstream across the hull surface or moved downstream to set the flow tangent to the hull at a number of points equal to the number of cylinders. This technique was not carried out because of the high curvature of the streamlines near the leading edge of the cylinders and because of the relatively small effect of the cylinders upon the duct thrust as found by the present analysis.

The present method of solution assumes potential flow. Therefore, when the duct lies within the hull wake, it appears to be a mathematical requirement that the hull wake vorticity be concentrated into discrete vortex sheets so that the flow around the duct surface remains a potential flow. That is, it does not seem possible to rely upon the present potential flow solution

if, mathematically, the duct is submerged within a distributed field of vorticity. The accurate machine program in use at DTMB for prediction of the flow field over hulls and their boundary layers has not been employed in the present analysis since the hull wake is represented as a displacement thickness therein, and this representation is valid only outside the actual wake.

As a test of the accuracy of the analytical representation of the hull and its wake, the radial velocity component v was computed by machine at three points near the analytical hull shape (Fig. 2(b)), but outside the boundary layer. A point source and line sink represented the hull, and a single vortex cylinder represented the hull wake (Fig. 4). The computed velocities are listed below where they are compared with more precise values computed at DTMB for the actual hull shape with its boundary-layer-displacement thickness included. It can be seen that the values are in agreement with 10 percent.

$\frac{x}{L}$	$\frac{r}{L}$	$\frac{v}{V}$ (DTMB)	$\frac{v}{V}$ =	$\frac{v_H}{V}$ (hull)	+ $\frac{v_W}{V}$ (hull wake)
0.4	0.120	-0.0292	-0.0321	-0.0325	0.0004
.2	.100	.0499	- .0501	- .0520	.0019
.1	.060	.0690	- .0618	- .0786	.0168

The hull-wake cylinder contributes significantly only to the last computed value of v/V which is at the point nearest the end of the hull. Recomputation with two and then with three vortex cylinders to represent the hull wake yields the following values for v/V, respectively, -0.0684 and -0.0667, which are satisfactorily close to the DTMB value of -0.0690. Thus, the present flow model appears to yield: (1) nearly the same flow pattern over the hull and its wake as the DTMB program; and (2) a potential flow representation of the flow within the wake so that the duct can be placed within it.

The Propeller

The propeller is represented as an actuator disk which extends across the duct and which is assumed to add a uniform axial velocity increment γ to the slipstream without imparting swirl. The trailing vorticity shed by the actuator disk is approximated by a single vortex cylinder of constant diameter D and constant strength γ extending downstream from the duct. The extension of this vortex cylinder upstream from the duct exit plane to the actuator disk

constitutes part of the duct-bound vorticity. When a hull wake cylinder extends through the actuator disk, the disk loading or pressure jump is smaller inside the cylinder then outside. Although the actuator disk is placed in the duct inlet for convenience, the present solution is independent of the location of the disk within cylindrical ducts (Ref. 3). It is believed that the solution remains valid even when the disk is located forward of the aft end of the hull. In this case the central part of the actuator disk, which is removed by the hull, is in effect replaced by the pressure jump acting upon the hull surface aft of the disk.

The Duct

The duct is represented by a distribution of bound vorticity γ_D which is specified such that there is no flow through the duct surface or across its trailing edge in the presence of the hull, wake, and propeller. Initially, the duct shape is restricted to a thin cylinder with a chord-to-diameter ratio of 1/2. Duct camber, taper, and increased chord are introduced later. The effect of duct thickness is neglected based upon the evaluation in Appendix D. The reduction in size of the propeller with the addition of duct thickness causes a shift of thrust from the propeller to the duct. This indirect effect can be evaluated from the results in Section 4.3.3.

With the foregoing assumptions, the problem consists of determining the vorticity distribution for the ducted propeller and the associated hull drag, duct thrust, and propeller thrust forces such that there is no flow through the hull and duct surfaces and there is no net force on the configuration. The forces are evaluated from velocities acting upon singularities (by a Lagally type of formulation) rather than from integration of surface pressure.

2.2 Description of Iterative Procedure

The presence of the ducted propeller causes a velocity through the hull. This velocity is eliminated by an iterative procedure. The conditions of no flow through the duct and force equilibrium are maintained during each step of this procedure. The steps are:

(1) A solution for the isolated hull and its wake is obtained with a net drag force on the hull. The velocity induced normal to the hull surface by the wake cylinder, or cylinders, is neglected in this and the remaining steps.

(2) A solution is obtained for the hull and its wake combined with a ducted propeller. The propeller disk loading is chosen so that there is no

net force on the configuration. The duct-bound vorticity is specified such that there is no flow across the duct surface or its trailing edge. The ducted propeller induces velocity across the hull surface which is neglected in this step.

(3) An incremental source-sink distribution is added to the hull centerline to cancel the velocity induced by ducted propeller through the hull surface in Step (2).

(4) An incremental bound and trailing vorticity distribution is added to the ducted propeller which cancels both the force on the configuration and the velocity across the duct surface and its trailing edge caused by Step (3).

Steps (3) and (4) are repeated until the solution converges.

The following interference forces are generated by the various components of the singularity distribution acting upon each other:

(1) Increased hull drag, or a "thrust deduction," is caused by the ring elements of duct-bound vorticity acting upon the source-sink distribution for the hull shape. An equal increase in duct thrust is also generated and there is no net force on the configuration from hull-duct interference. This is because each elementary source and ring vortex induce equal but opposite forces on each other.

(2) Increased hull drag is caused by the free vorticity in the ducted propeller slipstream acting upon the source-sink distribution.

(3) Duct thrust is generated by the free vorticity in the propeller slipstream and hull wake acting upon the duct-bound vorticity.

The strength of the free vortex cylinder trailing from the duct (and the corresponding propeller thrust) is determined such that the net thrust of the ducted propeller is equal to the net drag of the hull.

The solution for the first iteration (through Step (2)) is carried out in Section 3.2. This solution is complete in the sense that all of the forces generated by mutual interference are included. However, the solution satisfies the actual hull boundary condition only approximately, because the hull shape corresponding to the point source and line sink is not exact and this shape is distorted by both the hull wake cylinders and the ducted propeller. The distortion of the hull shape by the ducted propeller is examined in Section 3.3 where Step (3) of the interation procedure is carried out.

3. ANALYSIS FOR THIN CYLINDRICAL DUCTS

3.1 Specification of Configuration

To begin the analysis, we shall specify the hull shape and the vortex cylinders which represent its wake using the nomenclature of Figure 1.

The isolated hull shape of interest (TMB Model 4620, Ref. 1) can be represented in potential flow by the dividing streamline surrounding a point source and line sink of constant strength as shown in Appendix A. The submarine hull shape and propeller from Reference 1 are compared with the analytical hull shape in Figures 2(b) and 3. The analytical shape is found by fairing Equations (A.1) and (A.2) as described in Appendix A and using the following assumed parameters defined in Figure 1:

$$\frac{L_Q}{R_m} = \frac{93.87}{12.27} = 7.65$$

$$\frac{L_B}{R_m} = \frac{70}{12.27} = 5.72 \qquad (1)$$

The length-to-radius ratio of the hulls are

$$\text{actual} \quad \frac{L}{R_m} = \frac{180}{12.27} = 14.7$$

$$\text{analytical} \quad \frac{L}{R_m} = \frac{170}{12.27} = 13.8 \qquad (2)$$

The analytical hull shape near the aft end is compared in Figure 3 with a parabola for which

$$\frac{x}{L_B} = \left(\frac{r_B}{R_m}\right)^2 \qquad (3)$$

$$\pi R_m^2 = \frac{Q}{V} \qquad (4)$$

$$\frac{L_W}{L_B} = \left(\frac{R_W}{R_m}\right)^2 \qquad (5)$$

The foregoing approximate Equations (3), (4), and (5) will be used in the present analysis to specify the shape of the hull boattail. Now we shall

specify the strength and radii of the vortex cylinders which are to be used to represent the hull wake.

Axial velocity profiles measured aft of the isolated hull in Reference 1 are shown in Figure 4 together with the downstream profiles given by the vortex cylinders which will be used to represent the hull wake. Either one, two, or three vortex cylinders will be used, with the radii and strength indicated in Figure 4. The three-vortex cylinder configuration is also shown to scale in Figure 3.

The vortex cylinders were chosen to approximate the measured profiles and to give an isolated hull drag coefficient of

$$C_H' = 0.050 \tag{6}$$

The measured drag coefficient corresponding with the measured velocity profiles in Figure 4 was $C_H' = 0.057$ for a Reynolds number, based on hull length, of $Re = 2.4\times10^7$, according to information supplied by DTMB. Since the hull drag was largely due to shear, the hull drag coefficient scales roughly with $Re^{-1/5}$, and the value assumed by Equation (6) corresponds to $Re \approx 4.6\times10^7$. For a thin, cylindrical duct with $c/D = 1/2$ and for the hull and wake specified by Equations (3) through (6) and Figure 4, the geometric configuration of the hull and ducted propeller is determined by specification of two additional parameters defined in Figure 1.

$$\text{Hull-to-duct radius ratio, } \frac{R_m}{R} = R_m'$$

$$\text{Hull-to-duct spacing ratio, } \frac{S}{R} = S'$$

The radius of the standard open propeller in Reference 1 was $R_P = R_m/2.63$. The size and location of this propeller relative to the hull is indicated in Figure 3. Three different values of hull-to-duct radius ratio will be used in the following computations: 2, 2.63, and 4. The spacing ratio will be varied from $0 > S/R > 1$.

3.2 First Iteration - Neglecting Interference of Ducted Propeller on Hull Boundary Condition

To solve for the vorticity distributions and forces for the components of a specified geometric configuration, we shall first determine expressions for the radial velocity induced by each configuration component at the duct

surface. Then we shall require that the duct-bound vorticity distribution cancel this radial velocity such that the boundary condition of no-flow through the duct is satisfied. The form of the bound vorticity distribution will be specified such that there is no flow across the trailing edge of the duct in order to satisfy the Kutta condition. Finally, the propeller thrust will be specified such that the thrust of the ducted propeller equals the drag of the hull with interference.

3.2.1 Duct boundary condition

First we shall determine the radial velocity induced by the hull, represented by a point source-line sink, at the duct surface. Then we shall determine the radial velocity induced by the other configuration components.

Hull

The radial velocity induced at a point on the duct surface (x_Q,R) by the point source at the hull nose is

$$v_Q = \frac{Q}{4\pi} \frac{R}{\left(x_Q^2 + R^2\right)^{3/2}} \tag{7}$$

with the nomenclature defined in Figure 1. The stream function for the line sink used to represent the hull boattail is (p. 458, Ref. 2)

$$\psi = - \frac{Q}{4\pi L_B} \left(\sqrt{R^2 + x_B^2} - \sqrt{R^2 + (x_B - L_B)^2}\right)$$

Hence, the radial velocity induced by the line sink at a point on the duct (x_B,R) is

$$v_B = \frac{1}{R} \frac{\psi}{x_B} = - \frac{Q}{4\pi R L_B} \left(\frac{x_B}{\sqrt{R^2 + x_B^2}} + \frac{L_B - x_B}{\sqrt{R^2 + (x_B - L_B)^2}}\right) \tag{8}$$

Combining Equations (4), (7), and (8), gives the radial velocity at the duct due to the hull as

$$\frac{v_H}{V} = \frac{v_Q + v_B}{V} = \frac{R R_m^2}{4\left(x_Q^2 + R^2\right)^{3/2}} - \frac{R_m^2}{4RL_B} \left(\frac{x_B}{\sqrt{R^2 + x_B^2}} + \frac{L_B - x_B}{\sqrt{R^2 + (x_B - L_B)^2}}\right) \tag{9}$$

For cases of practical interest (where $R_m/R \geq 1$, and $x_Q/R_m \geq 10$) the first term, which represents v_Q/V, is smaller than 0.00025. Hence, we can neglect it and write

$$\frac{v_H}{V} = -\frac{(R_m')^2}{4L_B'}\left(\frac{x_B'}{\sqrt{1+(x_B')^2}} + \frac{L_B' - x_B'}{\sqrt{1+(x_B' - L_B')^2}}\right) \tag{10}$$

where, from Figure 1, we have

$$x_B = L_B + S + \frac{c}{2} + x_s$$

or

$$x_B' = L_B' + S' + \frac{c'}{2}(1 - \cos\theta) = L_B' + S' + c' \sin^2\frac{\theta}{2}$$

We shall expand Equation (10) in a Fourier series as

$$\frac{v_H}{V} = \sum_0^\infty F_n \cos n\theta \tag{12}$$

Values of the Fourier coefficients F_n as machine computed for two specific geometric configurations are listed in Table I.

Hull Wake

The radial velocity component induced at a point on the duct surface by each of the vortex cylinders which represent the hull wake can be found from Equation (A.5), Reference 3, as

$$\frac{v_{\gamma_W}}{\gamma_W} = \frac{v_{\gamma_W}}{fV} = -\frac{1}{\pi}\sqrt{\frac{R_W}{R}}\left(\frac{E-K}{k_W} + \frac{k_W}{2}K\right) \tag{13}$$

where, for each vortex cylinder,

$$\gamma_W = fV$$

$$k_W^2 = \frac{4R/R_W}{\left(1 + \frac{R}{R_W}\right)^2 + \frac{x_W^2}{R_W^2}}$$

$$x_W = L_W + S + \frac{c}{2} + x_s$$

$$= L_W + S + c \sin^2 \frac{\theta}{2}$$

Again, we shall expand Equation (13) in a Fourier series as

$$\frac{v_{\gamma_W}}{\gamma_W} = \sum_{o}^{\infty} A_n^* \cos n\theta$$

such that all of the hull wake cylinders induce the velocity

$$\frac{v_W}{V} = \sum_{o}^{\infty} \left(\sum^{z} f A_n^* \right) \cos n\theta = \sum_{o}^{\infty} A_n \cos n\theta \qquad (14)$$

Values of the Fourier coefficients A_n as machine computed for two specific geometric configurations are listed in Table I. It is evident from Table I that the radial velocity induced inward along the duct chord by the hull is much greater than that induced outward by the hull wake cylinder.

Actuator Disk

The radial velocity component induced at a point on the duct surface by the vortex cylinder shed from the actuator disk can be found from Equation (2), Reference 3, as

$$\frac{v_\gamma}{\gamma} = \sum_{o}^{\infty} B_n \cos n\theta \qquad (15)$$

The actuator disk is placed in the duct inlet for convenience since the duct thrust is independent of the disk location for a thin, cylindrical duct. The coefficients B_n are functions of only c/D and they are listed in Table II as they appear in Table I of Reference 3.

Duct

The radial velocity component induced at a point on the duct surface by the duct-bound vorticity can be found from any of References 3 through 7. If the chordwise distribution of duct-bound vorticity is expressed by a Glauert (or Birnbaum) series as

$$\frac{\gamma_D}{\gamma} = C_o \cot \frac{\theta}{2} + \sum_1^\infty C_n \sin n\theta \tag{16}$$

then the induced velocity can be written as

$$\frac{v_{\gamma_D}}{\gamma} = + \frac{C_o}{2} - \sum_{\ell=0}^{\infty} \frac{C_\ell}{2} P_{o\ell} + \sum_{k=1}^{\infty} \cos k\theta \left(- \frac{C_k}{2} + \sum_{\ell=0}^{\infty} \frac{C_\ell}{2} P_{k\ell} \right) \tag{17}$$

The $P_{k\ell}$ coefficients depend only upon c/D and are listed in Table II as they appear in Tables 2.1 through 2.4 of Reference 6 or Table I of Reference 3. For an isolated ducted actuator disk, composed of a thin, cylindrical duct and a uniformly loaded actuator disk across its inlet, the values of the first four C_n coefficients are listed in Table II as they appear in Table I of Reference 3. These values were found by setting $v_\gamma + v_{\gamma_D} = 0$ to satisfy the duct boundary condition.

The problem now consists of determining the C_n coefficients in Equation (16) such that the duct boundary condition is satisfied with interference, that is,

$$v_H + v_{\gamma_W} + v_\gamma + v_{\gamma_D} = 0 \tag{18}$$

We can write the preceding equation as

$$\frac{V}{\gamma} \left(\frac{v_H}{V}\right) + \frac{V}{\gamma} \left(\frac{v_W}{V}\right) + \left(\frac{v_\gamma}{\gamma}\right) + \left(\frac{v_{\gamma_D}}{\gamma}\right) = 0 \tag{19}$$

with the parenthesized terms give, respectively, by Equations (12), (14), (15), and (17) as

$$\frac{v_H}{V} = \sum_o^\infty F_n \cos n\theta \tag{20}$$

$$\frac{v_W}{V} = \sum_o^\infty A_n \cos n\theta \tag{21}$$

$$\frac{v_\gamma}{\gamma} = \sum_{o}^{\infty} B_n \cos n\theta \tag{22}$$

$$\frac{v_{\gamma_D}}{\gamma} = \frac{C_o}{2} - \sum_{k=o}^{\infty} \frac{C_\ell}{2} P_{o\ell} + \sum_{k=1}^{\infty} \cos k\theta \left(- \frac{C_k}{2} + \sum_{\ell=o}^{\infty} \frac{C_\ell}{2} P_{k\ell} \right) \tag{23}$$

Substitution of Equations (20) through (23) into (19), gives the following equations for the coefficients of the Fourier harmonics. For $n = 0$

$$\left.\begin{aligned} &\frac{V}{\gamma} (F_o + A_o) + B_o + \frac{C_o}{2} - \sum_{\ell=o}^{\infty} \frac{C_\ell}{2} P_{o\ell} = 0 \\ &\text{and for } n > 0 \\ &\frac{V}{\gamma} (F_n + A_n) + B_n - \frac{C_n}{2} + \sum_{\ell=o}^{\infty} \frac{C_\ell}{2} P_{n\ell} = 0 \end{aligned}\right\} \tag{24}$$

Later we shall truncate Equations (24) for the duct boundary condition after $\ell = 3$ and after $n = 3$. Then we shall have a set of four equations for the C_ℓ coefficients and the slipstream vorticity γ. To obtain the additional equation required for solution, we shall now consider the condition of thrust equilibrium.

3.2.2 Thrust equilibrium

We shall require that there be no net force on the complete geometric configuration so that with interference, the thrust on the ducted propeller is equal to the drag of the hull, or

$$T_{D(P)} + T_{D(H)} + T_{D(W)} + T_P = F_H + F_{H(P)} + F_{H(D)} \tag{25}$$

Since the duct-hull interaction forces cancel ($T_{D(H)} = F_{H(D)}$) we can write the foregoing equation in coefficient form as

$$C_{D(P)} + C_{D(W)} + C_P = C_H + C_{H(P)} = (R'_m)^2 \left[C'_H + C'_{H(P)} \right] \tag{26}$$

Next we shall derive expressions for the force coefficients in the foregoing expression.

Duct Thrust

For the assumed thin, cylindrical duct, the duct thrust force is due entirely to leading-edge suction, or the coefficient C_o of the first singular term in Equation (16). The thrust force can be expressed by analogy to a flat plate at angle of attack (Eq. (10), Ref. 3) as

$$T_D = \frac{\pi^2}{4} \rho c D (\gamma C_o)^2 \tag{27}$$

such that

$$C_D = \frac{T_D}{Aq} = 2\pi \frac{c}{D} \frac{\gamma^2}{V^2} C_o^2 \tag{28}$$

For the isolated ducted propeller, the duct thrust is generated by the propeller alone so that C_o is a function of only B_n. However, the presence of the hull and its wake effects the duct thrust, and for the present case, C_o is a function of F_n, A_n, and B_n as given by Equation (24).

Propeller Thrust

Without the effect of the hull wake, the propeller thrust can be found simply by use of Bernoulli's equation ahead of and behind the uniformly loaded actuator disk as

$$T_p = A_p \Delta p = A_p \frac{\rho}{2} \left(V_j^2 - V^2 \right) = A_p \frac{\rho}{2} (\gamma^2 + 2V\gamma) \tag{29}$$

If we assume uniform disk loading (or uniform pressure jump) with the vortex cylinders representing the hull wake extending through the actuator disk, each wake cylinder will change strength at the actuator disk. To avoid this complication, and to better represent the actual radial distribution of propeller loading, we shall assume that the actuator disk adds a uniform velocity increment γ to the slipstream which flows through it as indicated in Sketch B for one wake cylinder.

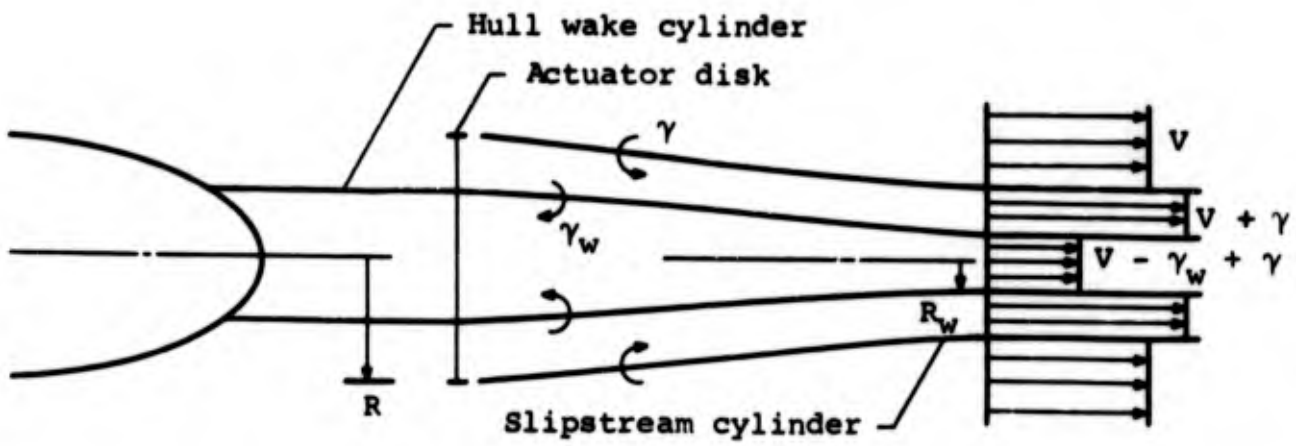

Sketch B.- Nomenclature for propeller thrust.

The disk loading (or total pressure jump) is thus smaller in the central part of the disk than in the outer part. To evaluate the disk loading we shall neglect the change in radius of the wake cylinder R_w with the addition of the actuator disk and with distance downstream of the disk. Then the disk loading can be found from the increased total pressure[1] in the slipstream which is produced by the actuator disk. That is, if $R_w < R$ as shown, then the propeller thrust force is given by

$$T_p = \pi R_w^2 \frac{\rho}{2} \left[(V - \gamma_w + \gamma)^2 - (V - \gamma_w)^2\right] + \pi \left(R^2 - R_w^2\right) \frac{\rho}{2} \left[(V + \gamma)^2 - V^2\right] \tag{30}$$

or

$$C_p = \frac{T_p}{\pi R^2 q} = \frac{\gamma^2}{V^2} + 2 \frac{\gamma}{V} Z \tag{31}$$

where

$$Z = 1 - \frac{\gamma_w}{V} = 1 - f \tag{32}$$

On the other hand if $R_w > R$ we find that C_p is given by Equation (31) but with

---

[1]This increased total pressure is equal to the static pressure jump across the actuator disk.

$$Z = 1 - f(R'_W)^2 \tag{33}$$

By similar reasoning we find that for two and three wake cylinders and for various relative sizes of the actuator disk, the propeller thrust coefficient is given by Equation (31) with the values of Z given in Table III.

Hull Drag

The hull drag force coefficient is considered to be composed of three parts:

(1) The frictional or shear drag coefficient C'_H which is assumed to equal the drag coefficient measured for the isolated hull.

(2) The profile drag coefficient $C'_{H(D)}$ (or thrust deduction) due to the interference of the duct on the hull.

(3) The profile drag coefficient $C'_{D(P)}$ due to the interference of the propeller on the hull.

The first drag coefficient C'_H is specified to equal 0.050 (see Section 3.1). The hull drag caused by duct interference, corresponding to $C_{H(D)}$, is equal to the duct thrust caused by hull interference $C_{D(H)}$. The latter force will be computed as the change in duct thrust produced by putting $F_n = 0$ in Equations (24).

An expression for the hull drag coefficient due to propeller interference $C_{H(P)}$ is developed in Appendix C as Equation (C.5). This drag is caused by the axial velocity distribution induced along the hull centerline by the vortex cylinder γ shed from the trailing edge of the ducted propeller. The foregoing velocity distribution acts upon the point source and line sink which represent the isolated hull and which are not affected by interference in the first iteration.

3.2.3 Governing equations and their solutions

Truncation of the duct boundary condition (Eqs. (24) after $\ell = 3$ and after $n = 3$) gives the following set of four equations for the four C_ℓ coefficients and for the strength of the slipstream vortex cylinder γ.

$$\left.\begin{aligned}
&\frac{V}{\gamma}(F_o + A_o) + B_o + \frac{1}{2}(+C_o - C_oP_{oo} - C_1P_{o1} - C_2P_{o2} - C_3P_{o3}) = 0\\
&\frac{V}{\gamma}(F_1 + A_1) + B_1 + \frac{1}{2}(-C_1 + C_oP_{1o} + C_1P_{11} + C_2P_{12} + C_3P_{13}) = 0\\
&\frac{V}{\gamma}(F_2 + A_2) + B_2 + \frac{1}{2}(-C_2 + C_oP_{2o} + C_1P_{21} + C_2P_{22} + C_3P_{23}) = 0\\
&\frac{V}{\gamma}(F_3 + A_3) + B_3 + \frac{1}{2}(-C_3 + C_oP_{3o} + C_1P_{31} + C_2P_{32} + C_3P_{33}) = 0
\end{aligned}\right\} \quad (34)$$

The $P_{k\ell}$ coefficients which are lined out in the foregoing equations are identically equal to zero (Table II). Substitution for the remaining $P_{k\ell}$ coefficients from Table II for $c/D = 1/2$ and solution for the leading Fourier coefficient C_o (from the first and third of Eqs. (34)) gives

$$C_o = -2.1592\left[B_o + \frac{V}{\gamma}(F_o + A_o)\right] + 0.0800\left[B_2 + \frac{V}{\gamma}(F_2 + A_2)\right] \quad (35)$$

Substitution of Equations (28) and (31) into the thrust equilibrium Equation (26) gives

$$\pi c' C_o^2 + 1 + 2Z\frac{V}{\gamma} = \left[C_H + C_{H(P)}\right]\frac{V^2}{\gamma^2} \quad (36)$$

Substitution of Equation (35) for C_o, Equation (6) for C_H, Equation (C.5) for $C_{H(P)}$, and Table III for Z into Equation (36) gives a quadratic equation to be solved for γ. Since the hull drag due to duct interference $(C_{H(D)})$ has not been included in Equation (36) the equal duct thrust due to hull interference must be excluded by letting $F_o = F_2 = 0$ in Equations (35) as mentioned previously. The solution then gives γ and the effective value $(C_o)_e$ without the effect of hull-duct interference. Using this value of γ and the proper (non-zero) values of F_o and F_2 in Equation (35), one can solve for the total value $(C_o)_t$. When inserted in Equation (38) the two values $(C_o)_e$ and $(C_o)_t$ give the "useful" and total duct thrust coefficients, respectively, or $C_{D(P)} + C_{D(W)}$ and $C_{D(P)} + C_{D(W)} + C_{D(H)}$. The difference $(C_{D(H)} = C_{H(D)})$ is the hull-duct interaction force coefficient.

3.2.4 Computed results

The computed results for four assumed duct configurations are listed in Table IV. For all of these configurations the hull shape is specified by Equations (1) and (6) and shown dashed in Figure 2(b). The duct is a thin

cylinder with a chord-to-diameter ratio $c/D = 1/2$. The hull-duct configuration is indicated in Figure 5 for Case 2. The number of vortex cylinders used to represent the hull wake is varied from one to three as indicated in Figure 4 and the case dash numbers in Table IV.

The results obtained for one wake cylinder are as follows. In Cases 1-1, 2-1, and 3-1 the duct size is increased, and the effectiveness of the duct in unloading the propeller, or the "useful" duct-to-propeller thrust ratio $(C_{D(P)} + C_{D(W)})/C_P$ decreases markedly. In Case 4 the intermediate-sized duct is moved forward over the hull and the effectiveness of the duct decreases, while the interference between the hull and duct $C_{H(D)} = C_{D(H)})$ increases. This interference is very large for all of the cases computed for cylindrical ducts.

In the previous cases for one vortex cylinder representing the hull wake, the strength of the cylinder was selected to be half the free-stream velocity. To investigate the sensitivity of the results to this choice, the strength is cut in half in Case 5 with the hull drag coefficient C_H held constant. Although there is a significant effect upon the results, the new wake cylinder no longer gives a reasonable approximation to the hull wake profile in Figure 4.

To obtain better approximations to the hull wake, the first four cases were recomputed with two and then with three vortex cylinders representing the wake. The results indicate that there is relatively little effect upon the force coefficients as the number of wake cylinders is increased from one to two and particularly from two to three.

3.3 Second Iteration - Including Interference from Ducted Propeller on Hull Boundary Condition

The foregoing results were obtained by neglecting the interference effect of the ducted propeller upon the hull boundary condition. This same approximation is discussed and used for an open (unducted) propeller in Reference 1. Because of this approximation the shape of the hull boattail is distorted by the presence of the ducted propeller. In Appendix B a series of point sources is added to the line sink which represents the boattail. The source strengths are specified such that the flow is tangent to the hull, and, hence, the hull-boundary condition is satisfied, at the axial station of each point. The calculations were carried out for Case 4 of Table IV. It is found that the strength of the sources alternate in sign and a rather ragged distribution of strength is required. Furthermore, the strength distribution

varies markedly between three arbitrarily assumed sets of point spacings and locations. Nevertheless, the results in Appendix B indicate that the addition of the point sources changes the combined force on the hull and duct by less than 3.5 percent. Hence, the initial approximation of neglecting the distortion of the hull boattail by the ducted propeller is retained throughout the present analysis. It should be noted, however, that even though it cancels out of the present analysis, the hull-duct interaction force increased about 17 percent because of the addition of the point sources.

4. ANALYSIS FOR THIN CAMBERED DUCTS

Here we shall include the effects of duct camber in the foregoing analysis for a thin, cylindrical duct.

4.1 Governing Equations and Their Solution

We shall place the duct-bound vorticity and satisfy the duct boundary condition on the "reference cylinder" of radius R, such that

$$v = v_H + v_W + v_\gamma + v_{\gamma_D} = V \frac{dr_s}{dx_s} \tag{37}$$

Only the radial components of velocity induced by the hull, wake, propeller, and duct are included in the foregoing equation. The axial components are assumed negligible compared with the free-stream velocity V. This may be a poor approximation when the duct is very near the hull or deep within the hull wake. We shall assume that the duct shape includes small amounts of camber as indicated in Sketch B, such that

$$\begin{aligned} \frac{dr_s}{dx_s} &= R_o + R_1 \cos\theta \\ &\quad + R_2 \cos 2\theta + R_3 \cos 3\theta \\ &= R_o + R_1 \cos\theta \\ &\quad + R_2(2\cos^2\theta - 1) \\ &\quad + R_3(4\cos^3\theta - 3\cos\theta) \end{aligned} \tag{38}$$

Integration of Equation (38) gives the cambered duct shape as

$$\frac{r_s - R}{c} = - R_o\left(\frac{1 + \cos\theta}{2}\right) + R_1\left(\frac{1 - \cos^2\theta}{4}\right) + R_2\left(\frac{1}{6} + \frac{1}{2}\cos\theta - \frac{1}{3}\cos^3\theta\right)$$
$$+ R_3\left(-\frac{1}{4} + \frac{3}{4}\cos^2\theta - \frac{1}{2}\cos^4\theta\right)$$

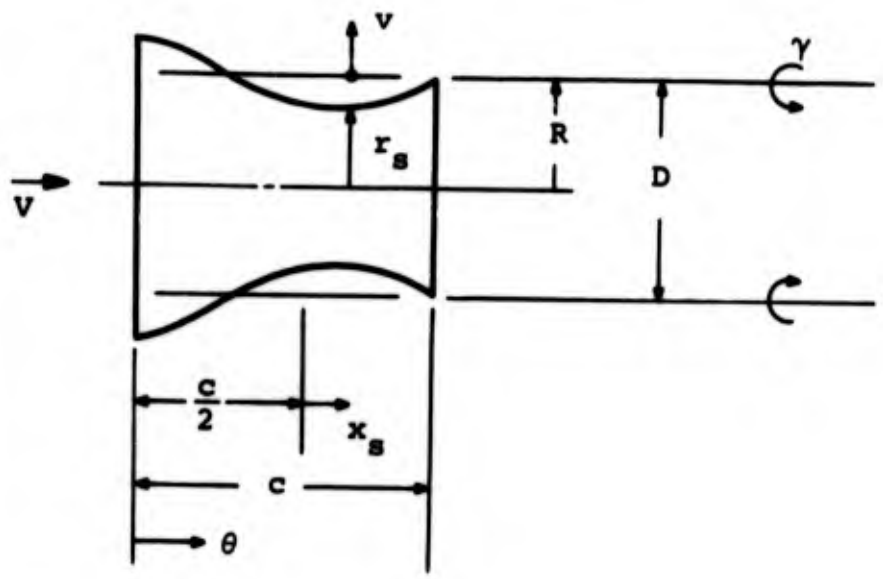

Sketch C.- Nomenclature for cambered duct.

If the actuator disk is in the duct inlet then the four components of induced radial velocity are given by Equations (20) through (23). Substitution of these expressions and Equation (38) into Equation (37) gives the following set of equations for the first four Fourier coefficients C_n when Equation (23) is truncated after C_3 as before. This set of equations is analogous to Equation (34) for a cylindrical duct.

$$\left.\begin{aligned}
&\frac{V}{\gamma}(F_o + A_o) + B_o + \frac{1}{2}(+C_o - C_oP_{oo} - C_2P_{o2}) = \frac{V}{\gamma}R_o \\
&\frac{V}{\gamma}(F_1 + A_1) + B_1 + \frac{1}{2}(-C_1 + C_oP_{1o} + C_1P_{11} + C_3P_{13}) = \frac{V}{\gamma}R_1 \\
&\frac{V}{\gamma}(F_2 + A_2) + B_2 + \frac{1}{2}(-C_2 + C_oP_{2o} + C_2P_{22}) = \frac{V}{\gamma}R_2 \\
&\frac{V}{\gamma}(F_3 + A_3) + B_3 + \frac{1}{2}(-C_3 + C_1P_{31} + C_3P_{33}) = \frac{V}{\gamma}R_3
\end{aligned}\right\} \quad (39)$$

The Fourier coefficients C_n can be determined by solving the first and third equations for C_o and C_2, then solving the second and fourth equations

for C_1 and C_3, and finally substituting for the $P_{k\ell}$ coefficients from Table II. The same expressions (except for truncation differences) can be obtained more directly from Equations (22) and (24) of Reference 7, when $c/D = 1/2$, as[2]

$$\left.\begin{aligned} C_0 &= -1.0796\ \epsilon_0 + 0.0400\ \epsilon_2 \\ C_1 &= -0.1719\ \epsilon_0 + 1.0933\ \epsilon_1 + 0.0064\ \epsilon_2 - 0.0138\ \epsilon_3 \\ C_2 &= -0.0274\ \epsilon_0 + 1.0179\ \epsilon_2 \\ C_3 &= +0.0009\ \epsilon_0 - 0.0046\ \epsilon_1 + 1.0062\ \epsilon_3 \end{aligned}\right\} \qquad (40)$$

where

$$\epsilon_n = 2B_n + 2\,\frac{V}{\gamma}\,(A_n + F_n - R_n) \qquad (41)$$

The duct-bound vorticity distribution (γ_D/γ) is now given by Equations (16) and (40) when the actuator disk is located in the inlet of the cambered duct. If the disk is put at any other axial station within the duct the total vorticity $(\gamma_D + \gamma)$ along the reference cylinder must remain fixed to maintain the duct boundary and Kutta conditions. Hence, we add γ to the duct-bound vorticity distribution (γ_D in Eq. (16)) upstream of the actuator disk location as it is moved back into the duct.

For the subsequent analysis we shall put the actuator disk across the exit plane of the duct. This can be done by changing the sign of the B_n coefficients when n is odd as indicated in Table II. Then Equation (15) gives v_γ/V and Equations (16) and (40) give the duct-bound vorticity γ_D/γ for the actuator disk in the exit plane.

The same duct-bound vorticity γ_D/γ could be obtained by the alternative procedure of using the previous B_n coefficients to solve for C_n in Equation (40), but then adding unity (γ/γ) to the right side of Equation (16) for γ_D/γ, that is, adding

$$1 + \frac{4}{\pi} \sum_{1,3,5,\ldots}^{\infty} \frac{\sin n\theta}{n} \qquad (42)$$

or adding $4/\pi n$ to the odd C_n coefficients.

---

[2]Similar expressions can also be found for $c/D = 1$.

The elementary thrust force on each ring vortex element of the duct-bound vorticity is given by

$$dT_D = -\rho\pi D \left(v_H + v_W + v_\gamma\right) \gamma_D \, dx_s \tag{43}$$

where v is a radial velocity induced at the ring element and $\gamma_D \, dx_s$ is the circulation about the ring. The duct-bound vorticity distribution γ_D has already been determined (Eqs. (16) and (40)) and the radial velocity induced at the ring element by the hull, hull wake, and propeller is given by Equations (20), (21), and (22), as

$$v_H + v_W + v_\gamma = \sum_1^\infty \left[(F_n + A_n)V + \gamma B_n\right] \cos n\theta \tag{44}$$

or as

$$\frac{v_H + v_W + v_\gamma}{\gamma} = \frac{1}{2} \sum_1^\infty \epsilon_n^* \cos n\theta$$

where

$$\epsilon_n^* = 2B_n + 2\frac{V}{\gamma}(A_n + F_n) = \epsilon_n + 2\frac{V}{\gamma} R_n \tag{45}$$

Substitution of Equations (16) and (44) into Equation (43) and integration over the duct chord gives the total thrust force on the duct as

$$T_{D(P)} + T_{D(H)} + T_{D(W)} = -\rho\pi D \frac{c}{4} \gamma^2 \int_0^\pi \sum_0^\infty \epsilon_n^* \cos n\theta \left(C_0 \cot\frac{\theta}{2} + \sum_1^\infty C_m \sin m\theta\right) \sin\theta \, d\theta \tag{46}$$

or

$$C_{D(P)} + C_{D(H)} + C_{D(W)} = -\pi \frac{c\gamma^2}{DV^2} \left[C_0(2\epsilon_0^* + \epsilon_1^*) + C_1\epsilon_0^* + \frac{1}{2}(C_2\epsilon_1^* + C_3\epsilon_2^* + \cdots) - \frac{1}{2}(C_1\epsilon_2^* + C_2\epsilon_3^* + \cdots)\right] \tag{47}$$

As before we shall truncate after C_3 and ϵ_3^*, and retain only the terms written in Equation (47). The hull-duct interaction coefficient $C_{H(D)} = C_{D(H)}$ is given by Equation (47) when $2(V/\gamma)F_n$ is substituted for ϵ_n^*.

The condition of thrust equilibrium is given by Equation (26) as

$$C_{D(P)} + C_{D(W)} + \frac{\gamma^2}{V^2} + 2\frac{\gamma}{V} Z = C_H + \frac{\gamma}{V} Y(R_m')^2 \qquad (48)$$

when C_H and Y can be obtained from Equations (6) and (C.5), Z is given by Table III, and the term $C_{D(P)} + C_{D(W)}$ is given by Equations (40), (41), (45), and (47), with $F_n = 0$. For a specified geometric configuration, the preceding equation is a quadratic equation for the single unknown γ/V. The machine solution consistently gives one positive and one negative root and no ambiguity for γ/V.

Evaluation of the terms appearing in Equation (47) by use of machine computed values indicates that the first two harmonics of duct camber (R_o and R_1) cannot be used to increase significantly the "useful duct thrust" without also obtaining impractically large amounts of either hull-duct interference or leading-edge suction. However, by including the higher harmonics (R_2 and R_3) one can obtain useful duct thrust with little interference and leading-edge suction. Although the interference force cancels from the present analysis, it is significant since it decreases the amount of useful duct thrust which can be obtained before the duct boundary layer separates.

4.2 Computed Results

The computational cases for cambered ducts are for the previous hull shape (Fig. 2(b)) and for thin ducts with the actuator disk extending across their exit planes. The size, location, and shape of the ducts are varied together with the number of vortex cylinders used to represent the hull wake.

The computed results for each case are: the ratio of propeller slipstream vorticity to free-stream velocity γ/V, the series coefficients for the duct-bound vorticity distribution (C_n in Eq. (16)), and finally the force coefficients for the various configuration components. The force coefficients are those appearing in Equation (26) which can be written as

$$C_P + C_{D(P)} + C_{D(W)} + C_{D(H)} = C_{H(D)} + C_H + C_{H(P)}$$

This equation specifies that there is no net force on the configuration, or that the thrust on the propeller plus the thrust on the duct is equal to the drag of the hull. The duct thrust is composed of the three components generated by the propeller, hull wake, and hull. The hull drag is that of the bare hull plus that generated by the duct and propeller. The terms $C_{D(H)}$ and $C_{H(D)}$ cancel. For the purpose of comparison, the ratio of "useful duct thrust" to propeller thrust, $\left[C_{D(P)} + C_{D(W)}\right]/C_P$, will be shown for each case together with the total duct thrust coefficient,

$$C_{D_t} = C_{D(P)} + C_{D(W)} + C_{D(H)}$$

and the duct thrust coefficient due to leading-edge suction

$$C_{D_s} = 2\pi \frac{c}{D}\left(C_o \frac{\gamma}{V}\right)^2 \tag{49}$$

The last coefficient is given by Equation (28) and it is equal to the total duct thrust for cylindrical ducts. For the cambered ducts C_{D_s} is computed by neglecting the increased length and slope of the duct leading edge due to camber. This is because the duct-bound vorticity is placed on the reference cylinder of radius R where the duct boundary condition is also satisfied.

A series of short duct shapes, with c = R, was computed first, followed by a series of longer ducts, with c = D. For all of these ducts, Table VI lists the assumed values which define the geometric configuration and the computed values which give the corresponding vorticity distribution for the ducted propeller. The duct configurations are shown plotted in Figures 5, 6, and 7, and the computed force coefficients are listed in Table VII. The results for the short ducts will be described first.

4.2.1 Results for short ducts, c = R

These cambered duct shapes are variations from the cylindrical duct shape computed previously as Case 2-2. The results of this case are shown as the first entry in Table VII, for comparison purposes.

Cases 6, 7, and 8

These cases show (Table VII) that duct camber can be used to decrease $C_{D(H)}$ and increase $C_{D(P)}$ simultaneously. However, the large amounts of duct camber assumed for these cases is beyond the range of practicality and

and beyond the range of validity for the present analysis. Furthermore, the duct leading-edge suction is excessively large.

Case 9

This duct has less camber, hull interference, and leading-edge suction. The "useful" duct-to-propeller thrust ratio is high and, hence, the performance of this duct is much better than that of the cylindrical duct.

Case 10

The duct camber is reduced by half. The "useful" duct-to-propeller thrust ratio decreases by less than half. The hull interference reverses sign but remains small. The duct leading-edge suction becomes very small. It will be shown in Section 4.3.3 that when the actuator disk is located in the duct throat the "useful thrust" of this duct increases appreciably.

Cases 11

These cases are for a duct shape similar to Case 9 but with less curvature near the exit plane. The "useful duct thrust" is less than for Case 9. The effect of changing the number of vortex cylinders which represent the hull wake is small, particularly between two and three cylinders.

Case 12

From Case 11-2 the duct is moved forward on the hull by one chord length. All of the effects are unfavorable. The hull-duct interference reverses sign and becomes very large. This result indicates that by traversing the duct axially the interference can be nulled out.

Case 13

The duct size is decreased from Case 11-2. The "useful duct thrust" increases somewhat, but the hull-duct interference and the duct leading-edge suction both increase much more.

4.2.2 Results for long ducts, c = D

The longer ducts are shown in Figures 6 and 7, and the computed force coefficients are listed in the last half of Table VII. The cambered duct shapes are variations from the cylindrical duct of Case 14. The size of the duct relative to the hull is held constant at $R/R_m = 0.38$.

Case 14

The cylindrical duct has extremely large total thrust and leading-edge suction. Nearly all of this thrust is caused by hull-duct interference; however, the "useful duct thrust" is small and negative (i.e., unuseful duct drag).

Case 15

The duct camber line is the same as for Cases 11 through 13 except that it has been "stretched" forward over the hull boattail. The duct performance is much improved over the cylindrical duct.

Case 16

The duct is moved aft by half its chord length. The "useful duct thrust" increases slightly, the leading-edge suction becomes small, and the hull-duct interaction force changes sign. Hence, this case indicates again that the interaction force can be nulled by traversing the duct. The results for Cases 15 and 16 for the longer ducts compare qualitatively with Cases 12 and 11 for the shorter ducts, but the effectiveness of the longer ducts is slightly less.

Case 17

The duct shape and location are the same as for Case 15 except that the camber is increased by 6/5. The same effects occur for Cases 16 and 17.

Case 18

The duct camber line is nearly the same as for the shorter duct of Case 9. The "useful duct thrust" is slightly greater for the longer duct, but the leading-edge suction and hull-duct interference are several times larger so that the longer duct is less favorable.

Case 19

The duct is bowed inward slightly from Case 18 as indicated in Figure 6. The main effect is that the interference forces on the duct from both the hull and its wake both change sign. Hence, both of these forces can be reduced nearly to zero simultaneously by bowing duct 18 inward about 1/3 as much as for Case 19. The duct leading-edge suction remains high compared with the shorted duct, however.

Cases 20, 21, 22, and 23

The shape of the duct camber line is the same for these cases, but the amount of camber is increased as shown in Figure 7. The duct inlet is made slightly converging to decrease the leading-edge suction. For duct 21 both two and three vortex cylinders are used to represent the hull wake with very little difference in the results. The force coefficients for these cambered ducts and the uncambered duct are plotted in Figure 8. It can be seen that between Cases 21 and 23 all of the interferer. forces, $C_{D(P)}$, $C_{D(H)}$, $C_{H(D)}$, and $C_{D(W)}$, are small. Hence, the bare hull drag C_H nearly equals $C_D + C_{D(P)}$. Of particular interest is the fact that the flow over the duct leading-edge also reverses as indicated in Figure 8 and by the sign of C_o in Table VI. Hence, the duct leading-edge suction is very small for both Cases 21 and 23 and is nearly zero for an intermediate duct shape 22.

4.2.3 Effect of putting the actuator disk at the duct throat

The foregoing results for cylindrical ducts are independent of the axial location of the actuator disk within the duct if it is downstream of the hull. The results for the cambered ducts are for the actuator disk in the duct exit plane. All of the cambered duct shapes (Figs. 5, 6, and 7) have been selected so that there is some expansion near the aft end of the duct. This was done to permit an increase in the "useful" duct-to-propeller thrust ratio by placing the actuator disk at the duct throat.

If the actuator disk is moved forward from the duct exit plane, there is no change in the vorticity distribution and flow field which have been computed. However, the disk area is reduced slightly at the duct throat, and the pressure jump across the disk acts upon the expanding duct area downstream of the throat. The incremental thrust force on the annular area $\pi(R^2 - R_p^2)$ acts upon the duct rather than the actuator disk when the disk is moved to the duct throat. The incremental thrust force is given by the annular area times the jump is total pressure across the annular part of the disk,[3] or

$$\Delta T = \pi \left(R^2 - R_p^2\right) \frac{\rho}{2} \left[(V - \gamma_W^* + \gamma)^2 - (V - \gamma_W^*)^2\right] \qquad (50)$$

where γ_W^* is the sum of the strength of the vortex cylinders in the hull wake with radius $R_W > R$. It is assumed that there are no wake cylinders

[3]This jump in total pressure is equal to the jump in static pressure since the fluid velocity is continuous across the disk.

crossing the duct surface between R_p and R. The corresponding incremental thrust coefficient is

$$\Delta C_T = \frac{\Delta T}{\pi R^2 q} = \left(1 - \frac{R_p^2}{R^2}\right)\frac{\gamma}{V}\left(2 - 2\frac{\gamma_W^*}{V} + \frac{\gamma}{V}\right) \tag{51}$$

For Case 9 we find from Figure 5 and Tables VI and VII

$$\frac{\gamma}{V} = 0.128, \quad \frac{\gamma_W^*}{V} = 0, \quad \frac{C_{D(P)} + C_{D(W)}}{C_P} = \frac{0.161}{0.207} = 0.78$$

Thus, if the actuator disk is moved from the duct exit plane to the duct throat where $R_p = 0.92R$ we find from Equation (51) that the incremental thrust coefficient which is subtracted from C_P and added to $C_{D(P)}$ is

$$\Delta C_T = 0.042$$

and the ratio of useful duct-to-propeller thrust becomes

$$\frac{C_{D(P)} + C_{D(W)}}{C_P} = \frac{0.161 + 0.042}{0.207 - 0.042} = \frac{0.203}{0.165} = 1.23$$

Hence, the ratio of useful duct thrust to propeller thrust increases from 0.78 to 1.23 as the actuator disk is moved to the duct throat.

Similarly, we find the values listed below for the cases indicated.

Case	$\frac{\gamma}{V}$	$\frac{\gamma_W^*}{V}$	$\frac{R_p}{R}$	ΔC_T Eq. (51)	$\frac{C_{D(P)} + C_{D(W)}}{C_P}$	
					Disk at exit plane	Disk at throat
9	0.128	0	0.92	0.042	0.78	1.23
10	.156	0	.96	.027	.46	.63
11-2	.154	0	.93	.094	.47	.78
21-2	.140	0	.94	.037	.62	.93
21-3	.140	0.1	.94	.034	.62	.89
22	.131	0	.93	.039	.74	1.13

With three vortex cylinders representing the hull wake in Case 21-3, the outer cylinder lies outside the duct exit plane. This has little effect upon the computed results as shown by comparison with Case 21-2. For Cases 21-2 and 22 the effect of moving the actuator disk to the duct throat is shown in Figure 8.

5. DISCUSSION OF RESULTS

All of the computed results are for the analytical hull shape shown in Figure 2(b) which is assumed to have an isolated drag coefficient and wake velocity profile comparable to measured data for TMB Model 4620 in Reference 1. Although the assumed hull wake and drag correspond to fixed values of hull Reynolds number and speed, the analysis should be applicable over a limited speed range since the hull wake and drag are insensitive functions of Reynolds number. The vorticity in the hull wake is concentrated into multiple (one, two, or three) vortex cylinders extending downstream from the hull boattail. The propeller is approximated by an actuator disk which extends across the duct and which adds a uniform velocity increment to the flow through it. The size, location, and shape of the duct is varied. The effect of duct profile thickness upon the duct thrust is neglected based upon the results in Appendix D. The velocity induced by the ducted propeller through the analytical hull shape is neglected based upon Reference 1 and Appendix B which indicate that there is relatively little effect upon the net force on the hull-duct combination. For the foregoing conditions the following results were obtained for three types of duct shapes: short cylindrical, short cambered, and long cambered.

5.1 Short Cylindrical Ducts

The results listed in Table IV indicate that:

(1) The hull-duct interaction force, $C_{H(D)} = C_{D(H)}$, is large. In some cases it is as large as the isolated hull drag C_H, and it is always larger than the duct thrust generated by the propeller $C_{D(P)}$.

(2) The hull drag caused by the propeller $C_{H(P)}$, is between 10 and 20 percent of the isolated hull drag C_H.

(3) The hull wake causes a duct drag, $C_{D(W)}$, which is as great as 40 percent of the duct thrust generated by the propeller $C_{D(P)}$.

(4) The duct is effective in unloading the propeller only for the smallest ducted propeller (Case 1). For this case the total duct thrust

$C_{D(H)} + C_{D(P)} + C_{D(W)}$, is nearly equal to the propeller thrust C_p. However, most of the duct thrust is canceled by hull interaction so that the "useful duct thrust" $C_{D(P)} + C_{D(W)}$, in only about 1/4 as large as the propeller thrust, C_p, even for the smallest duct.

5.2 Short Cambered Ducts, c = R

For short cambered ducts such as those shown in Figure 5, the results listed in the first half of Tables VI and VII indicate that:

(1) By cambering the duct one can markedly increase the effectiveness of the duct in unloading the propeller and simultaneously markedly decrease both the leading-edge suction on the duct and the interference of the duct with the hull and its wake. This can best be seen by comparison of Cases 9 and 11-2 with Case 2-2 for intermediate size ducts (and for small ducts by comparison of Case 13 with Case 1-2).

(2) The cambered duct shapes have been chosen such that there is some expansion near the duct exit plane. By moving the actuator disk forward from the duct exit plane to the duct throat, the effectiveness of the duct increases significantly as shown in Section 4.3.3. For example, the ratio, of useful duct thrust-to-propeller thrust $C_{D(P)} + C_{D(W)}/C_P$ increases from 0.08 to 0.47 with the introduction of duct camber for Case 11-2 and then increases again to 0.78 with the placement of the actuator disk at the duct throat.

(3) A duct camber line can be selected so that both the hull-duct interaction force and the duct leading-edge suction are small to avoid separation of the flow from the hull and duct lip. However, for the camber-line shapes assumed herein, the flow can separate from the aft part of the duct (from either the inner or outer duct surface) when the duct thrust is large. Experimental data for ducted propellers have indicated that the propeller blades are effective in mixing the duct boundary layer and delaying flow separation from the inner duct surface. Thus, it appears desirable to obtain duct thrust from the aft part of the duct rather than from leading-edge suction to avoid flow separation. The duct camber-line shapes assumed herein seem attractive from this point of view.

(4) The choice of the best duct camber-line shape depends upon the size and location of the duct relative to the hull and the chord-to-diameter ratio of the duct. For example, ducts 11 and 13 have the same shape but different size. However, if each of these duct shapes were optimized (for minimum interference and maximum effectiveness), the shapes would become different.

(5) There is little effect upon the final results of the number of vortex cylinders used to represent the hull wake (Cases 11).

5.3 Long Cambered Ducts, c = D

All of these ducts have the same size relative to the hull ($R_m = 2.63R$). The first series of long ducts have the same camber-line shapes as the shorter ducts "stretched" over a longer chord length, as shown in Figure 6. The results for the equivalent long and short ducts are qualitatively similar but the performance of the short ducts is slightly more favorable.

By small alteration of the duct camber-line and/or the hull-duct spacing the interference of the duct with the hull and hull wake can be reduced to zero simultaneously with little effect upon the duct effectiveness. However, the duct leading-edge suction remained relatively high for the long duct shapes shown in Figure 6.

The results for the long cambered ducts in Figure 7 show that there is a duct shape (duct 22) for which the duct interference with the hull and its wake and the duct leading-edge suction are all nearly zero. The fact that the leading-edge suction can be reduced to zero may be significant in the consideration of the duct boundary layer. The effectiveness of this duct in unloading the propeller is relatively high, however. In fact, if the propeller is located in the duct throat the computed ratio of "useful" duct thrust-to-propeller thrust is $C_{D(P)} + C_{D(W)}/C_P = 1.13$.

It is shown again (Case 21) that there is very little effect upon the final results of changing the number of vortex cylinders in the hull wake from 2 to 3.

6. CONCLUSIONS

Based upon the foregoing analytical results the following conclusions are drawn:

(1) Cylindrically shaped ducts are not suitable for shrouding a propeller mounted at the stern of the assumed hull shape. At cruising speed such a duct is relatively ineffective in unloading the propeller but it causes a large interference drag force on the hull which is canceled by an equally large thrust force on the duct due to leading-edge suction.

(2) By including a fairly large amount of duct camber, one can design the duct to have little interference with the hull and its wake and little leading-edge suction but large "useful thrust." For the assumed hull

(Fig. 2(b)) the shape of such a duct is indicated by duct 22 in Figure 7. If the propeller is placed in the throat of this duct the duct thrust can be greater than that of the propeller at cruising speed. For a more pointed hull boattail as indicated by the dashed line in Figure 7, somewhat less duct camber would probably be required.

(3) The results indicate that considerable control over the pressure distribution on the hull boattail can be obtained by suitable cambering of the duct. The effect of this change in pressure distribution on the hull boundary layer is neglected in the present analysis. However, it may be possible to retard boundary-layer growth and separation from the boattail with a suitably designed duct. The same considerations apply to the duct boundary layer as well.

(4) The main analytical approximations are neglecting duct profile thickness, neglecting the flow induced by the ducted propeller through the analytical hull surface, concentrating the vorticity in the hull wake into a few vortex cylinders, and satisfying the duct boundary condition at the reference cylinder. These approximations seem to be justified for the purpose of the present first analysis to estimate forces on the hull duct and propeller with mutual interference. However, it seems possible to extend and improve the analysis in several respects as indicated in the following section.

7. RECOMMENDATIONS FOR FUTURE WORK

The following recommendations are made for extending and improving the present analysis:

(1) To improve the analytical representation of an arbitrarily specified hull shape (e.g., TMB Model 4620) a source-sink distribution over the hull surface can be determined by modification of the accurate machine program which is in use at DTMB. With this machine program and the iterative procedure described in Section 2.2, the condition of no flow through the specified hull surface could be satisfied.

(2) Analytical expressions for both the axial and radial velocity components induced at a general field point by a vortex cylinder are now available (Ref. 9). With these expressions it appears practical to place the duct-bound vorticity and to satisfy the duct boundary condition at the cambered duct surface rather than at the reference cylinder. It also appears practical now to include the axial component of induced velocity in the boundary condition. Each of these modifications seems desirable for highly cambered ducts (such as duct 22 in Fig. 7).

(3) After the present analysis has been improved by the foregoing procedure, the boundary layer on the duct could be computed by use of available machine programs, for example, Reference 10. It seems essential to include consideration of frictional drag and flow separation on the duct in any procedure to optimize the duct design. For the boundary-layer computation the details of the duct pressure distribution as affected by the profile thickness of the duct will be needed.

(4) The final step in the program would appear to be an experimental verification of the analytical results. An optimum duct for propulsion of a specified underwater hull could be designed and tested. The performance of the system could be predicted for comparison with test data.

REFERENCES

1. Beveridge, J. L.: Effect of Axial Position of Propeller on the Propulsion Characteristics of a Submerged Body of Revolution. DTMB Rep. 1456, Mar. 1963.

2. Milne-Thompson, L. M.: Theoretical Hydrodynamics. The Macmillan Co., New York, 1960.

3. Kriebel, A. R.: Static Coefficients, Dynamic Stability Derivatives, and Interference for Ducted Propellers. Vidya Rep. 112, Mar. 31, 1964.

4. Weissinger, J.: Zür Aerodynamic der Ringflügels in Inkompressibler Strömung, Zeitschrift für Flugwissenschaften, Heft 3/4. pp. 141-150, Mar./Apr. 1956.

5. Ladurner, O.: Theoregical Investigation by Measuring Tests in What a Degree the Economy of Flying Vehicles is Influenced by Pre-Cambered Skeletons of Airfoils Closed in Themselves. Bureau Technique Zbrowski, DA-91-508-EUC 393, Aug. 1959, ASTIA No. AD 227082.

6. Ordway, D. E. and Greenberg, M. D.: General Harmonic Solutions for the Ducted Propeller. TAR-TR 613, Term, Inc., Ithaca, New York, Aug. 1961.

7. Hough, G. R.: The Aerodynamic Loading on Streamlined Ducted Bodies. Therm, Inc., Ithaca, New York, presented at Eighth Midwestern Mechanics Conference, Cleveland, Ohio, Apr. 1963.

8. Küchemann, D. and Weber, J.: Aerodynamics of Propulsion. McGraw Hill Book Co., Inc., New York, 1953.

9. Hough, G. R. and Ordway, D. E.: The Generalized Actuator Disk. TAR-TR 6401, Therm, Inc., Ithaca, New York, Jan. 1964.

10. Smith, A. M. O. and Clutter, D. W.: Solution of the Incompressible Laminar Boundary-Layer Equations. AIAA Jour., vol. 1, no. 9, Sept. 1963.

TABLE I

COMPUTED FOURIER SERIES COEFFICIENTS FOR RADIAL VELOCITY INDUCED AT DUCT

Case	$\frac{R_m}{R}$	$\frac{R_W}{R}$	n	For hull F_n (Eq. (12))	For hull wake A_n (Eq. (14))
1	4	1.270	0	-0.10532	0.006497
			1	- .06229	.002675
			2	- .00821	.000353
			3	.00023	.000038
			4	.00029	.000003
			5	.00004	- .000001
3	2	.632	0	- .05243	.007192
			1	- .03112	.004446
			2	- .00410	.000865
			3	.00011	.000130
			4	.00015	.000017
			5	.00002	.000002

Above results are for

$$\frac{L_B}{R_m} = 5.72, \quad \frac{c}{D} = \frac{1}{2}, \quad S = 0$$

and one wake cylinder with

$$\frac{R_W}{R_m} = 0.316, \quad \frac{\gamma_W}{V} = \frac{1}{2}$$

TABLE II

COMPUTED FUNCTIONS OF DUCT CHORD-TO-DIAMETER RATIO

$\frac{1}{2}c' = \frac{c}{D}$	$\frac{1}{4}$	$\frac{1}{2}$	1
$-B_0$ (a)	0.3531	0.2462	0.1771
$\pm B_1$	.3116	.2951	.2593
$-B_2$	.1617	.1643	.1643
$\pm B_3$	.1078	.1080	.1096
P_{00} (b)	.02683	.07281	.16016
P_{02}	.01343	.03644	.07907
P_{10}	.05366	.14561	.32032
P_{11}	.02987	.08526	.20609
P_{13}	.00304	.01252	.04629
P_{20}	.00608	.02491	.09186
P_{22}	.00403	.01655	.06338
P_{30}	-.00005	-.00016	.00402
$-P_{31}$	.00101	.00417	.01544
P_{33}	.00148	.00609	.02592
C_0 (c)	.7212	.5400	.3923
$-C_1$	↓	.5563	.4823
$-C_2$	↓	.3204	.3124
$-C_3$	↓	.2151	.2158

(a) The minus (plus) sign is for the actuator disk in the duct inlet (exit) plane. The even B_n coefficients are the same for both disk locations.

(b) The coefficients $P_{k\ell} = 0$ if $\ell > 0$ and $k + 1$ is odd.

(c) The C_n coefficients are for the actuator disk in the duct inlet.

TABLE III

VALUES OF Z FOR PROPELLER THRUST COEFFICIENT (Eq. (31)) FOR VARIOUS HULL WAKE CYLINDER COMBINATIONS

		Z
1. One wake cylinder 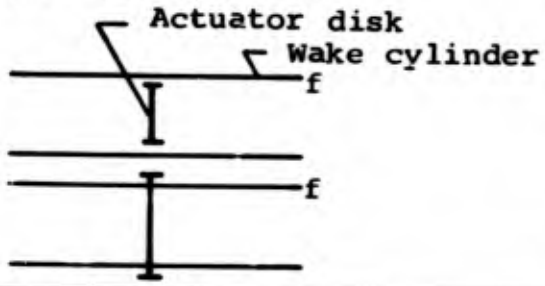	$R'_W < 1$	$1 - f$
	$R'_W > 1$	$1 - f(R'_W)^2$
2. Two wake cylinders 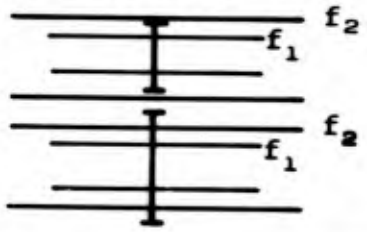	$R'_{W_1} < 1 < R'_{W_2}$	$1 - f_2 - f_1 \left(R'_{W_1}\right)^2$
	$R'_{W_1} < R'_{W_2} < 1$	$1 - f_2 \left(R'_{W_2}\right)^2 - f_1 \left(R'_{W_1}\right)^2$
3. Three wake cylinders 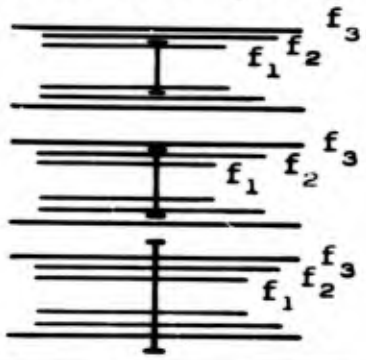	$R'_{W_1} < 1 < R'_{W_2} < R'_{W_3}$	$1 - f_3 - f_2 - f_1 \left(R'_{W_1}\right)^2$
	$R'_{W_1} < R'_{W_2} < 1 < R'_{W_3}$	$1 - f_3 - f_2 \left(R'_{W_2}\right)^2 - f_1 \left(R'_{W_1}\right)^2$
	$R'_{W_1} < R'_{W_2} < R'_{W_3} < 1$	$1 - f_3 \left(R'_{W_3}\right)^2 - f_2 \left(R'_{W_2}\right)^2 - f_1 \left(R'_{W_1}\right)^2$

TABLE IV

COMPUTED RESULTS FOR THIN CYLINDRICAL DUCTS WITH $c = R$, AND FOR THE HULL SHAPE IN FIGURE 2(b)

Case[1]	$\frac{R}{R_m}$	$\frac{S}{R}$	$\frac{R_W}{R}$	$\frac{\gamma_W}{V}$	$\frac{\gamma}{V}$	C_P	C_H	$C_{H(P)}$	$C_{D(P)}$	$C_{D(W)}$	$C_{D(H)} = C_{H(D)}$	$\frac{C_{D(P)} + C_{D(W)}}{C_P}$
1-1	0.25	0	1.26	0.50	0.493	0.736	0.800	0.136	0.222	-0.022	0.521	0.272
1-2	↓	0	↓	↓	.411	.776	.800	.122	.178	- .033	.468	.187
1-3		0			.485	.760	.800	.131	.207	- .036	.494	.225
2-1	.38	0	.832	.50	.228	.350	.346	.040	.048	- .011	.170	.104
2-2	↓	0	↓	↓	.208	.354	.346	.037	.040	- .011	.159	.082
2-3		0			.204	.355	.346	.036	.038	- .011	.156	.076
3-1	.50	0	.632	.50	.121	.208	.200	.016	.013	- .006	.075	.038
3-2	↓	0	↓	↓	.114	.208	.200	.015	.012	- .005	.074	.035
3-3		0			.113	.208	.200	.015	.012	- .005	.074	.035
4-1	.38	-1/2	.832	.50	.244	.379	.346	.066	.055	- .022	.346	.087
4-2	↓	-1/2	↓	↓	.222	.379	.346	.060	.045	- .018	.337	.070
4-3		-1/2			.217	.380	.346	.059	.043	- .019	.330	.063
5-1	.38	-1/2	.957	.25	.362	.358	.346	.058	.121	- 035	.451	.238

[1]The case dash number indicates the number of vortex cylinders used to represent the hull wake.

TABLE V

COMPUTED VALUES FOR EFFECT OF DUCTED PROPELLER ON HULL BOUNDARY CONDITION FOR CASE 4-1 OF TABLE IV

$Q = \pi R_m^2 V$, $L_B' = 15$, $C_P' = 0.055$, $C_H' = 0.050$, $C_{H(D)}' = 0.050$, $C_{H(P)}' = 0.096$

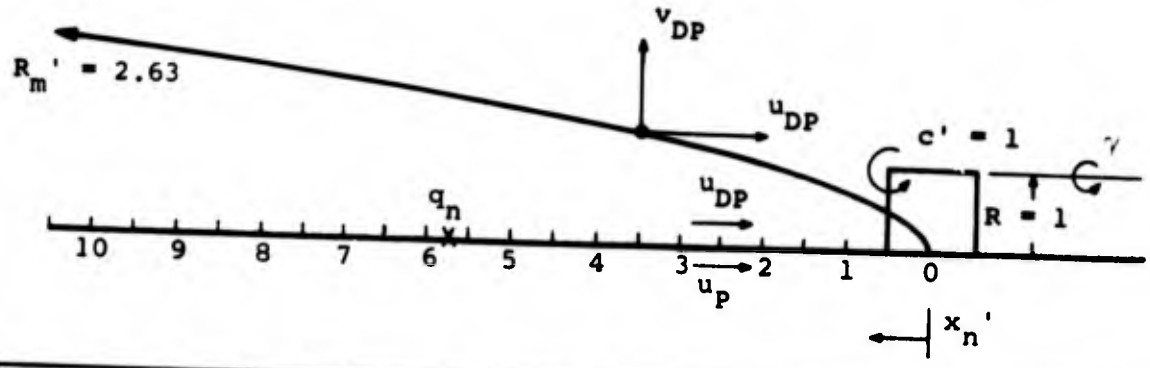

x_n'	At Hull Surface		At Centerline		q_n'		
	$\frac{u_{DP}}{V}$	$\frac{v_{DP}}{V}$	$\frac{u_{DP}}{V}$	$\frac{u_P}{V}$	Case 4-1-A	Case 4-1-B	Case 4-1-C
0.25	0.343	0.006	0.344	0.0490	-0.0085	-0.0070	-0.0128
.50	.361	- .003	.320	.0346	- .0020	- .0057	
.75	.301	- .096	.273	.0267	- .0339	- .0270	- .0166
1	.160	- .105	.209	.0204	.0262	.0143	
1.25	.105	- .082	.151	.0160	.0180	.0376	.0275
1.50	.063	- .049	.104	.0128	.0032	- .0281	
1.75	.046	- .033	.075	.0105	- .0317	.0190	- .0028
2	.033	- .023	.054	.0088	.0521	- .0340	
2.25	.026	- .016	.040	.0073	- .0416	.1153	.0006
2.50	.020	- .012	.030	.0061	.0168	- .2838	
2.75	.015	- .009	.025	.0057		.5680	.0038
3	.011	- .007	.022	.0050		- .9867	
3.25	.008	- .005	.019	.0044		1.5121	- .0044
3.50	.006	- .004	.017	.0038		-1.9904	
3.75	.005	- .003	.016	.0034		2.1808	.0056
4	.004	- .002	.015	.0030		-1.9180	
4.25	.003	- .001	.014	.0027		1.2973	- .0038
4.50	.002	- .001	.013	.0024		- .6315	
4.75	.001	0	.012	.0022		.1961	.0028
5	.001	0	.010	.0021		- .0297	
5.25	0	0					- .0036
5.75	↓	↓					.0029
6.25							- .0020
6.75							.0011
7.25							- .0007
7.75							.0004
8.25							- .0002
8.75							- .0001
9.25							0
9.75							0
				$\sum q_n'$	- .0013	- .0013	- .0018
				$\Delta C_{H(DP)}'$	.0105	.0093	.0098
				$\Delta C_{H(P)}'$	.0012	- .0019	.0013

TABLE VI

PROPELLER SLIPSTREAM VORTICITY AND SERIES COEFFICIENTS OF DUCT-BOUND VORTICITY (Eq. (18)) FOR THIN CAMBERED DUCTS (Eq. (38)) AND FOR THE HULL SHAPE IN FIGURE 2(b)

Case[1]	$\frac{c}{R}$	$\frac{R}{R_m}$	$\frac{S}{R}$	P_o	R_1	R_2	R_3	$\frac{\gamma}{V}$	C_o	C_1	C_2	C_3
2-2	1	0.38	0	0	0	0	0	0.208	1.184	0.444	- 0.350	0.217
6				0.3	0	1.5	-1	.110	6.540	.711	-27.991	18.511
7				.1	0	1.5	-1	.112	2.572	.099	-27.530	18.145
8				.1	0	1	-1	.126	2.672	217	-16.519	16.224
9				0	0	1	-1	.128	.948	-.042	-16.284	15.952
10				0	0	.5	-0.5	.156	.682	1.499	- 6.073	6.460
11-1				0	0	1	0	.135	.932	.192	-15.431	.219
11-2								.154	.879	.267	-13.576	.218
11-3								.151	.881	.262	-13.826	.218
12			-1					.179	1.816	.486	-11.566	.222
13		.25	0					.346	.897	.434	- 6.222	.217
14	2	.38	-1	0	0	0	0	.230	1.460	.371	- .207	.284
15			-1	0	0	.5	0	.165	1.263	-.043	- 6.677	.311
16			0	0	0	.5	0	.155	.329	.087	- 7.369	.197
17			-1	0	0	.6	0	.154	1.194	- 156	- 8.524	.318
18				0	0	.6	-5	.126	1.377	-.851	-10.409	8.517
19				0	-0.2	.6	- .5	.127	1.369	3.141	-10.324	8.384
20				-0.05	- .15	.30	- .25	.161	.794	1.900	- 4.263	3.489
21-2				- .07	- .21	.42	- .35	.140	.336	2.849	- 6.728	5.413
21-3				- .07	- .21	.42	- .35	.140	.307	2.881	- 6.697	5.407
22				- .08	- .24	.48	- .40	.131	.055	3.414	- 8.183	6.553
23				- .1	- .3	.6	- .5	.114	-.625	4.747	-11.604	9.230

[1]Two vortex cylinders represent the hull wake except as denoted by the case dash number. The actuator disk is across the duct exit plane. The assumed duct configurations are plotted in Figures 5. 6. and 7.

TABLE VII

FORCE COEFFICIENTS COMPUTED FOR CASES LISTED IN TABLE VI

Case[1]	C_P	C_H	$C_{H(P)}$	$C_{D(P)}$	$C_{D(W)}$	$C_{D(H)} = C_{H(D)}$	$\frac{C_{D(P)} + C_{D(W)}}{C_P}$	C_{D_s}	C_{D_t}
2-2	0.354	0.346	0.037	0.040	-0.011	0.159	0.082	0.19	0.19
6	.176		.019	.215	- .026	.240	1.07	1.58	.43
7	.180		.020	.184	.002	- .017	1.03	.26	.19
8	.203		.022	.173	- .009	.078	.81	.35	.24
9	.207		.023	.156	.005	- .050	.78	.05	.11
10	.256		.027	.118	- .001	.056	.46	.03	.17
11-1	.268		.024	.107	.005	- .058	.38	.05	.05
11-2	.253		.027	.113	.006	- .050	.47	.06	.07
11-3	.255		.027	.124	.007	- .051	.46	.05	.08
12	.300		.080	.156	- .030	.282	.42	.33	.21
13	.577	.800	.096	.326	- .008	.104	.55	.30	.41
14	.396	.346	.041	.069	- .079	.718	-.024	.71	.71
15	.274		.029	.111	- .010	.083	.37	.27	.18
16	.256		.015	.093	.012	- .108	.41	.02	-.003
17	.274		.029	.111	- .010	.083	.37	.27	.18
18	.203		.002	.154	.011	- .122	.81	.19	.14
19	.205		.022	.143	- .020	.243	.79	.19	.41
20	.265		.028	.134	- .025	.271	.41	.10	.38
21-2	.228		.025	.146	- .004	.101	.62	.014	.24
21-3	.229		.025	.149	- .007	.097	.62	.012	.24
22	.212		.023	.151	.006	.017	.74	.0003	.17
23	.184		.020	.156	.026	- .147	.99	.032	.035

[1]Two vortex cylinders represent the hull wake except as denoted by the case dash number. The actuator disk is across the duct exit plane.

BLANK PAGE

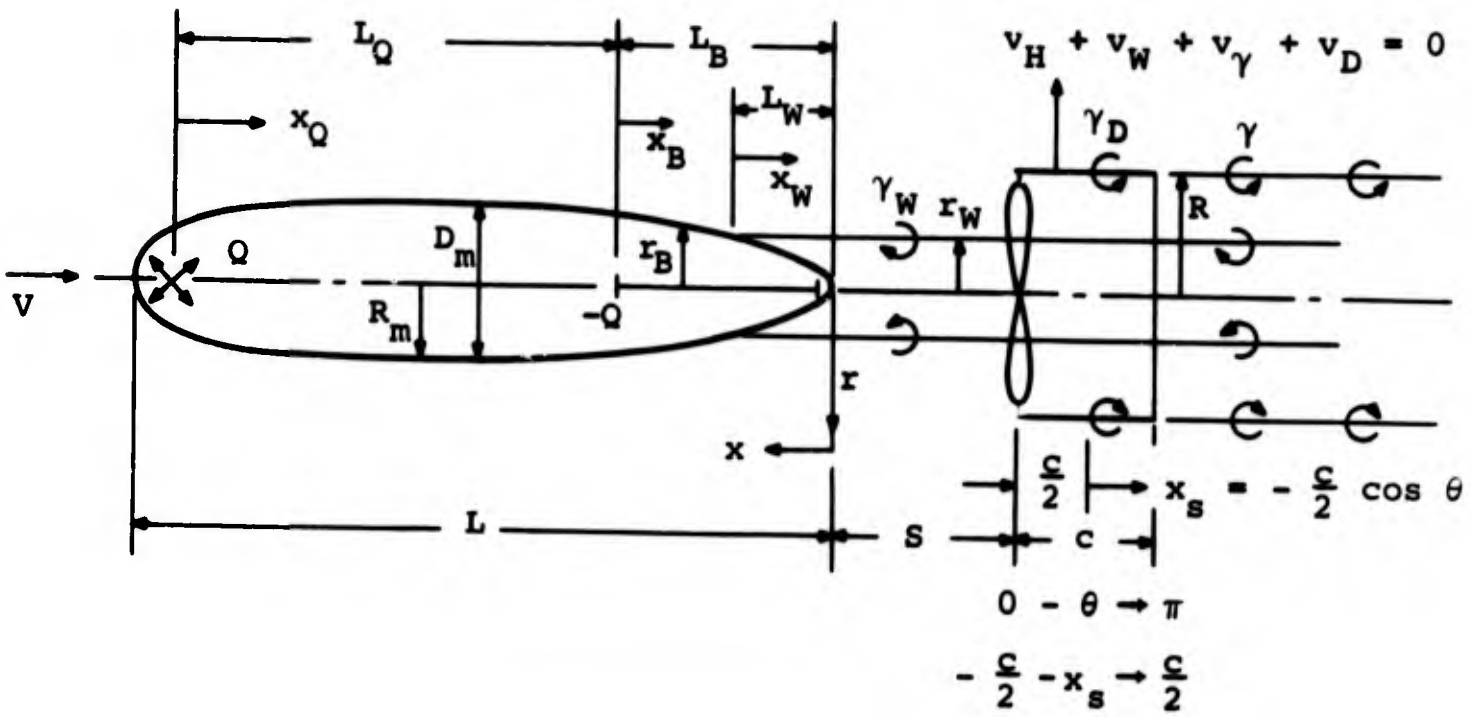

Figure 1.- Nomenclature for the hull and cylindrical ducted propeller.

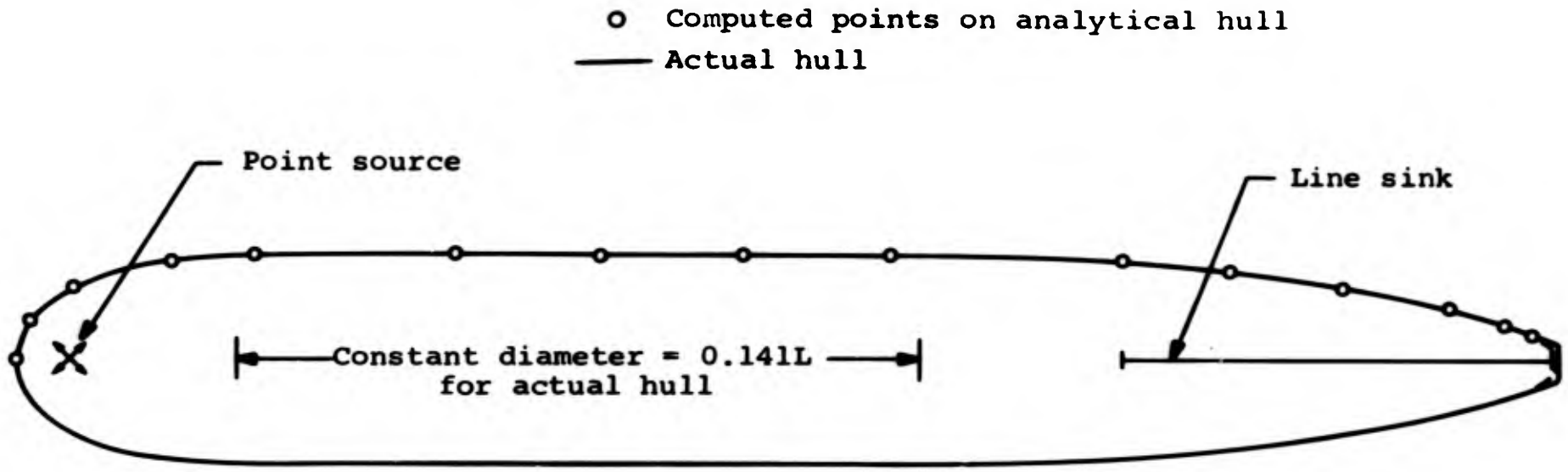

(a) Comparison of torpedo hull shape with points computed for point source and line sink.

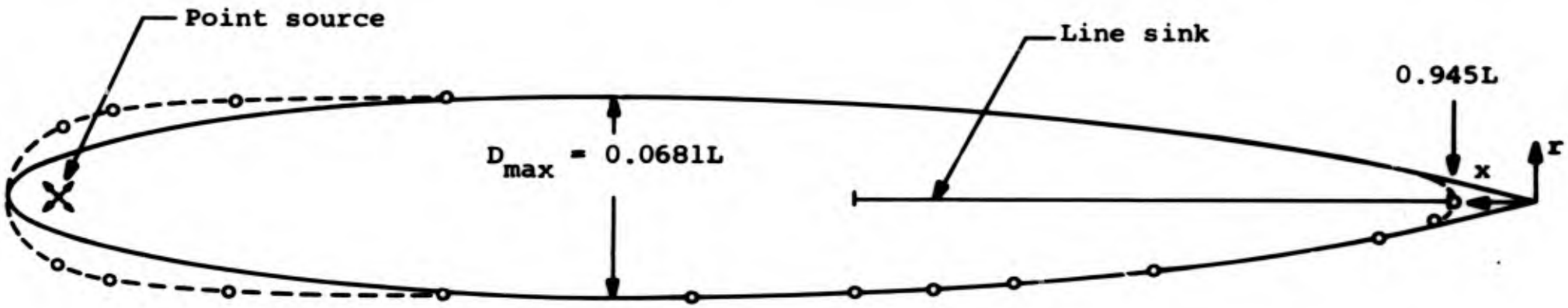

(b) Comparison of actual submarine hull shape (TMB Model 4620, Ref. 1) with points computed for point source and line sink.

Figure 2.- Comparison of actual and analytical hull shapes.

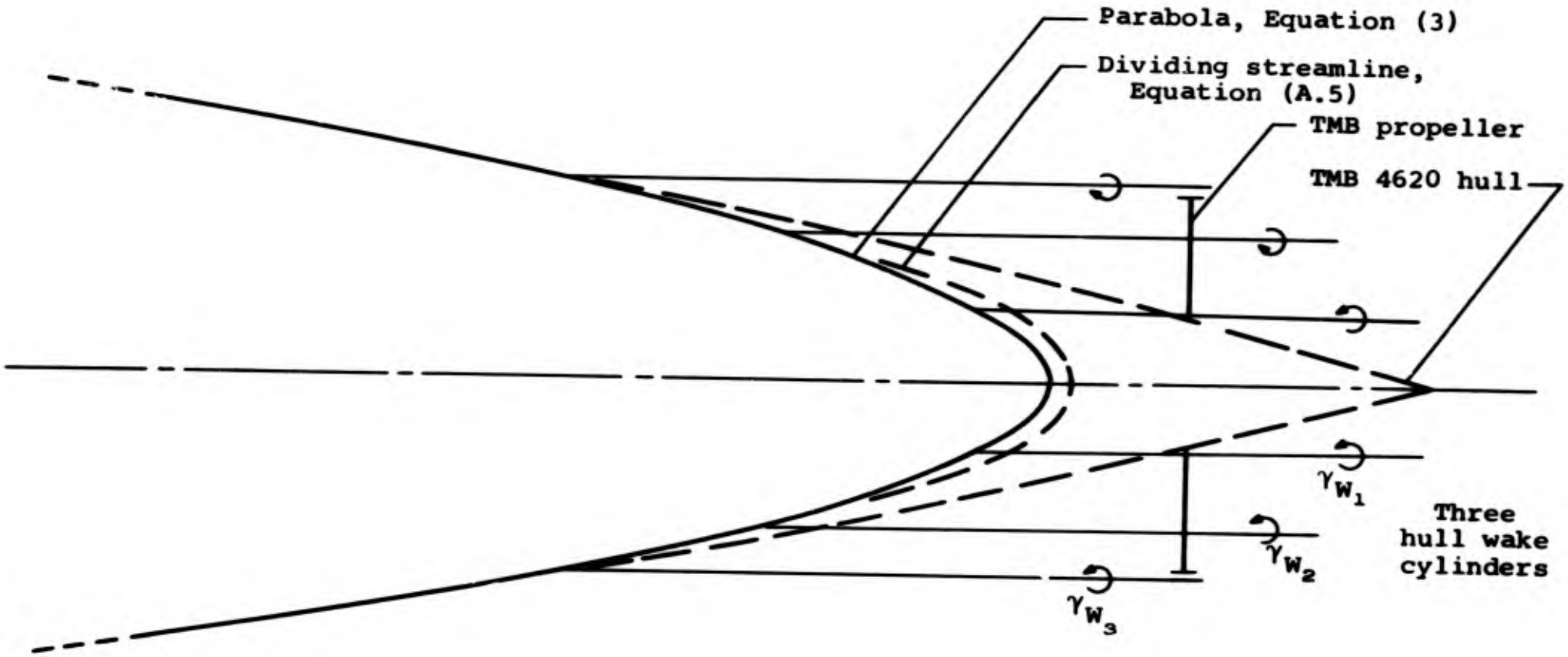

Figure 3.- Hull boattail and three vortex cylinders representing hull wake.

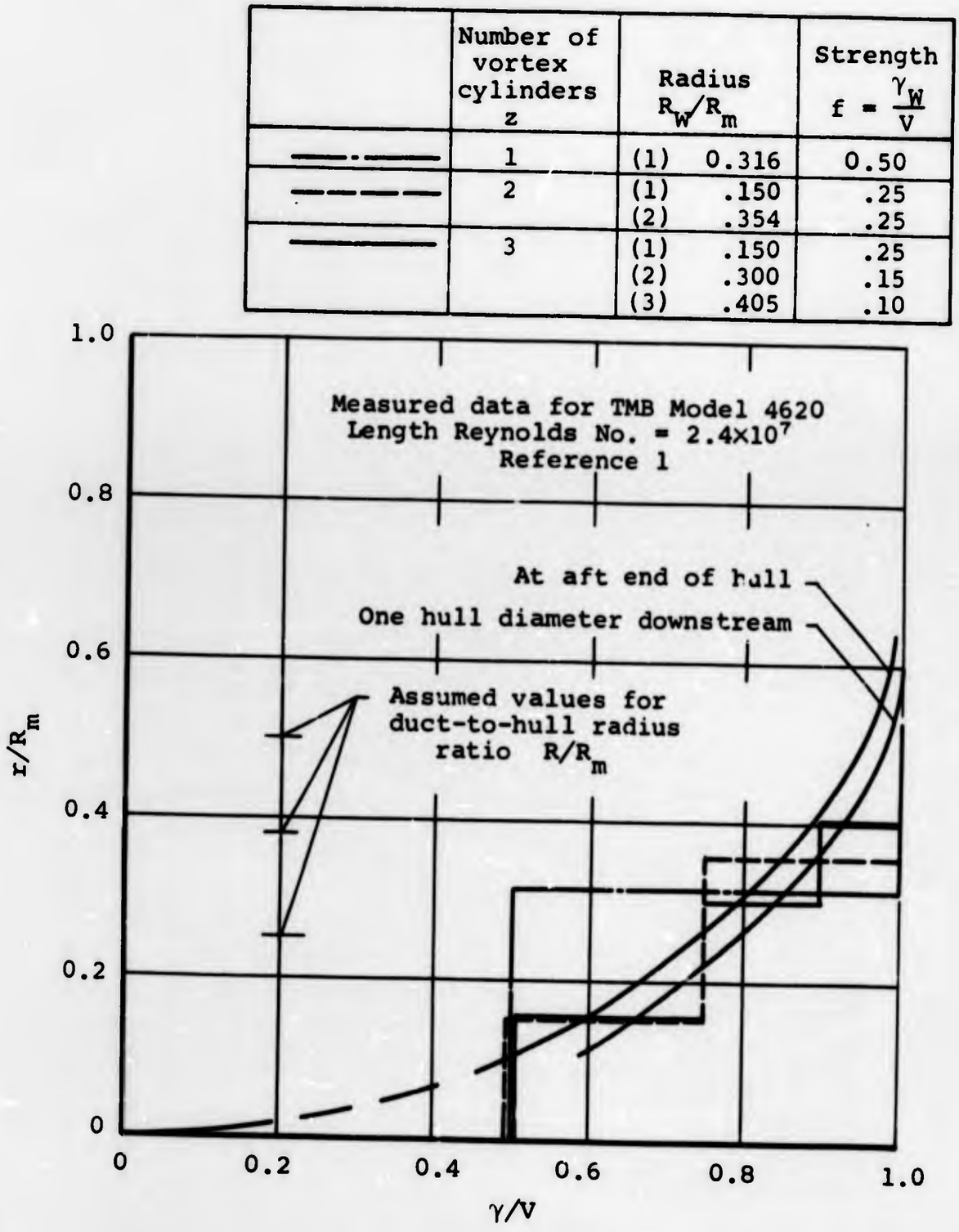

Figure 4.- Axial velocity profiles measured aft of TMB 4620 hull and analytical approximations from vortex cylinders.

BLANK PAGE

Case	$\frac{T_{D(P)}}{T_P}$	$\frac{T_{D(W)}}{T_P}$	$\frac{T_{D(H)}}{T_P}$	$\frac{T_{D_s}}{T_P}$
2-2	0.11	-0.03	0.45	0.96
6	.12	- .15	1.36	8.98
9	.75	.02	- .24	.24
11	.44	.02	- .20	.24

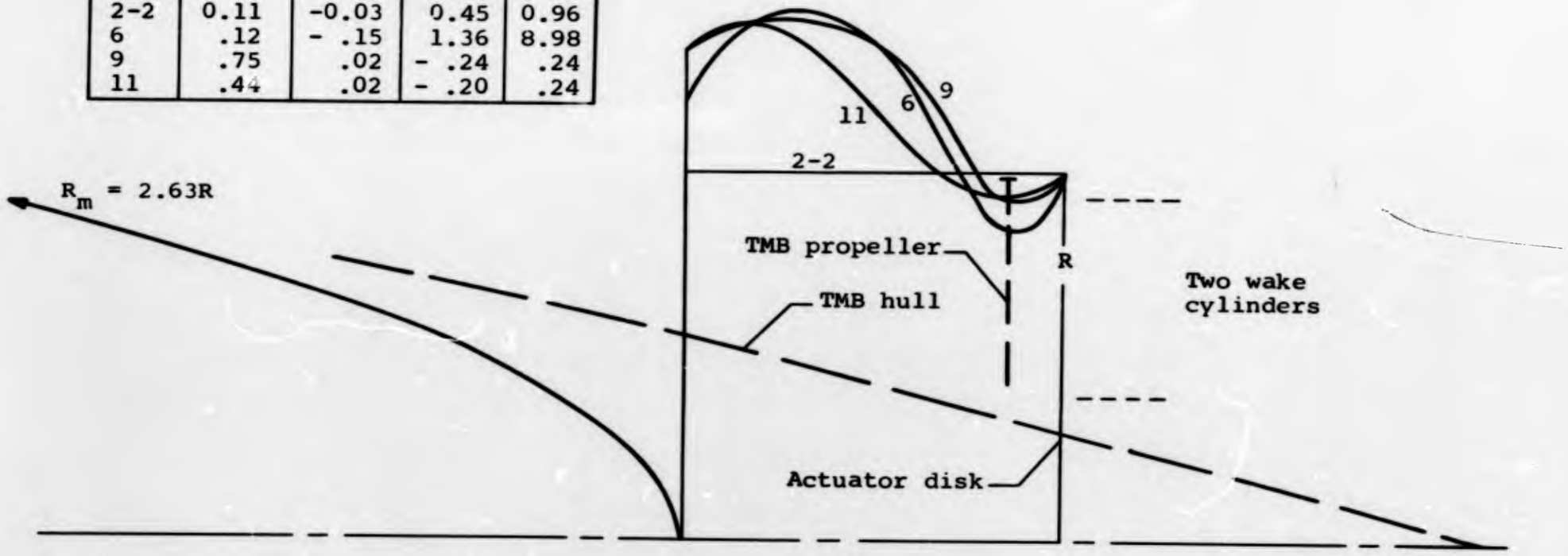

Figure 5.- Short cambered duct shapes with c = R.

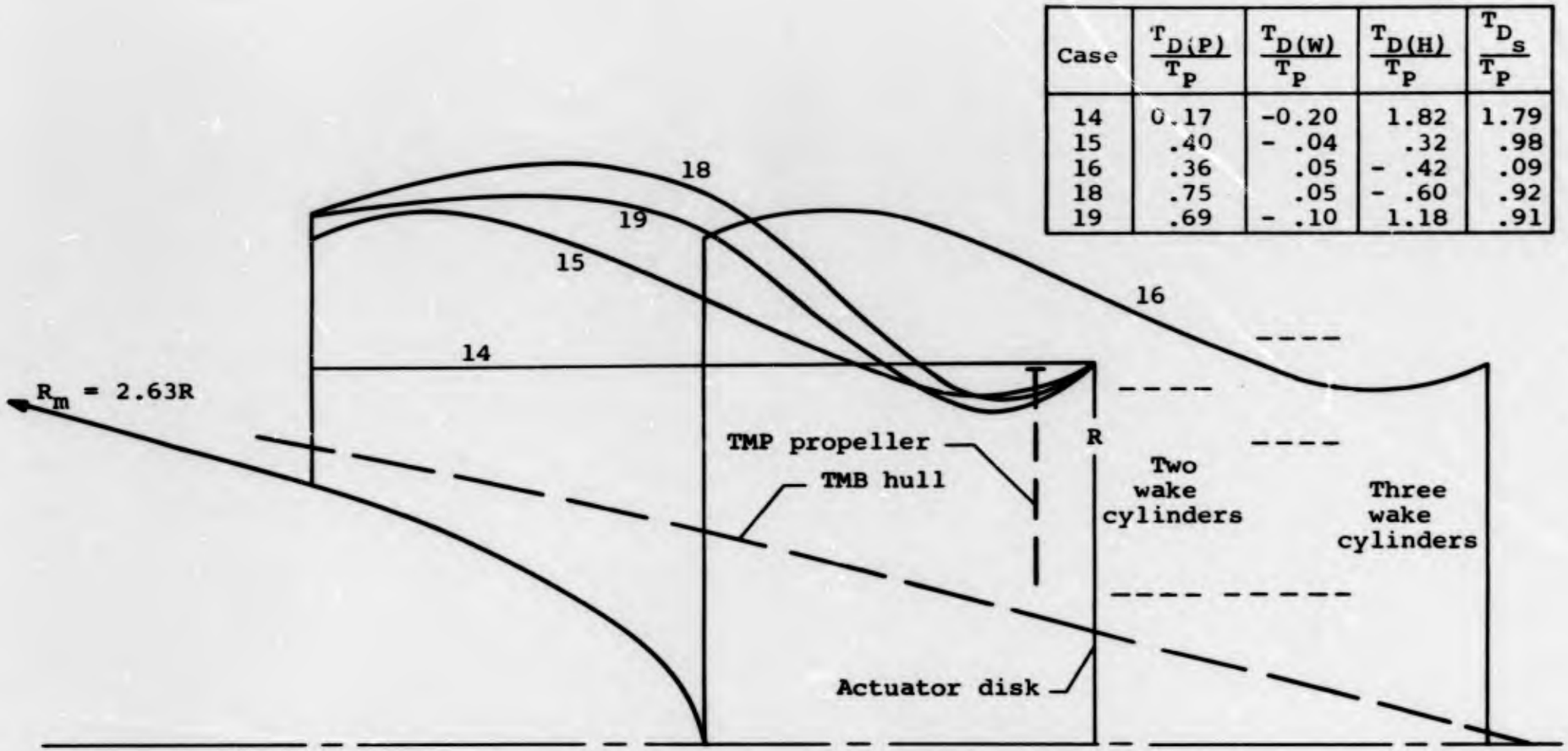

Case	$\frac{T_{D(P)}}{T_P}$	$\frac{T_{D(W)}}{T_P}$	$\frac{T_{D(H)}}{T_P}$	$\frac{T_{D_s}}{T_P}$
14	0.17	-0.20	1.82	1.79
15	.40	- .04	.32	.98
16	.36	.05	- .42	.09
18	.75	.05	- .60	.92
19	.69	- .10	1.18	.91

Figure 6.- Long cambered duct shapes with c = D.

Case	$\frac{T_{D(P)}}{T_P}$	$\frac{T_{D(W)}}{T_P}$	$\frac{T_{D(H)}}{T_P}$	$\frac{T_{D_s}}{T_P}$
14	0.17	-0.20	1.82	1.79
20	.50	- .09	1.02	.10
21	.64	- .02	.44	.06
22	.71	.03	.08	.0003
23	.85	.14	- .80	.03

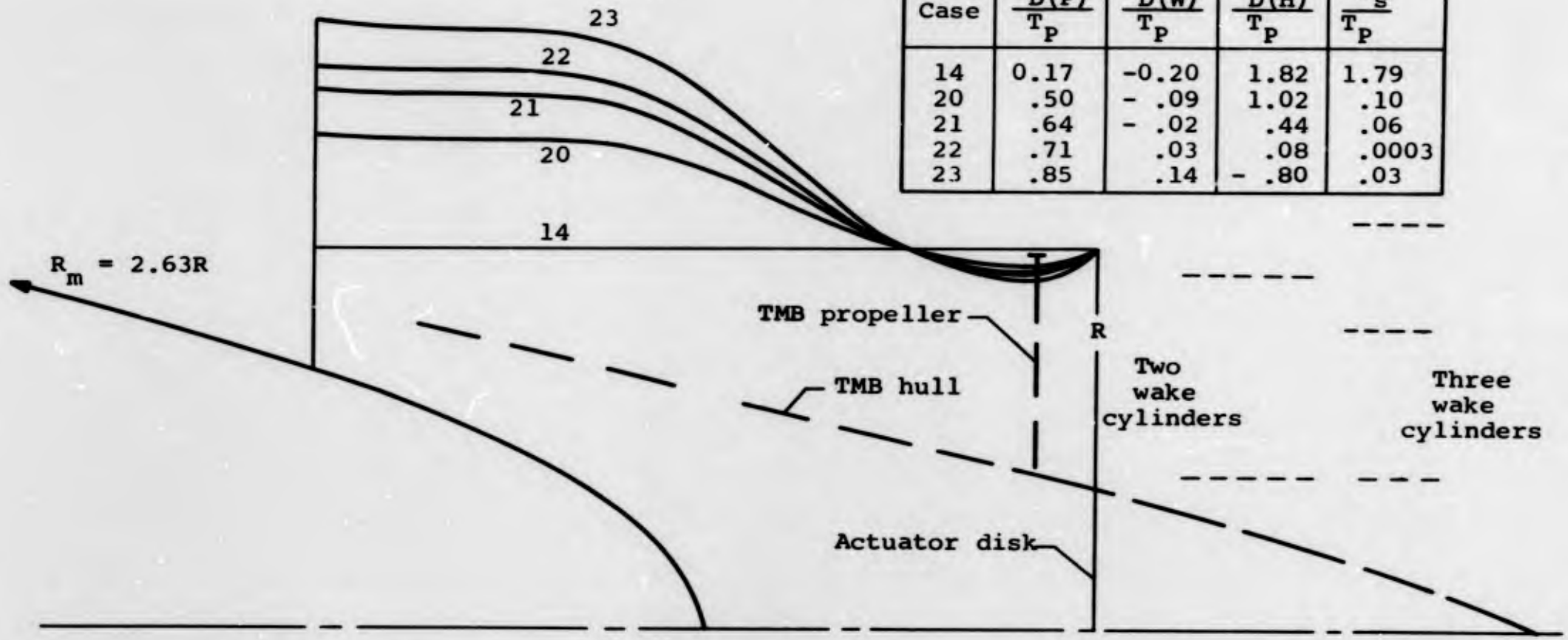

Figure 7.- Long cambered duct shapes with c = D.

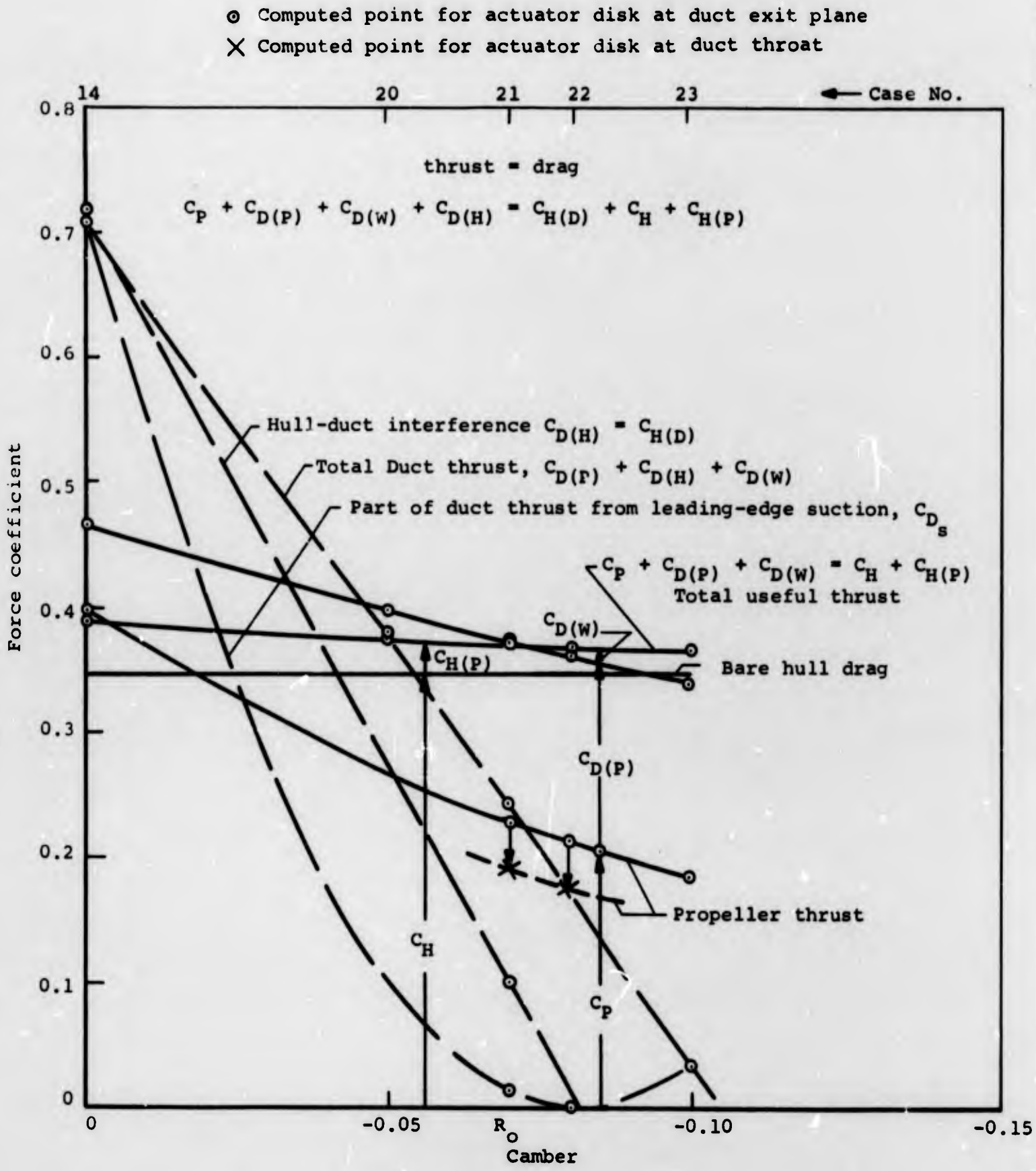

Figure 8.- Comparison of force coefficients for long cambered ducts in Figure 7.

APPENDIX A

ANALYTICAL REPRESENTATION OF THE HULL

Here we shall derive a technique for estimating the dividing streamline in the potential flow over a point source followed by a line sink of uniform strength. Then we shall compare such "hull shapes" with both torpedo hull and the submarine hull of interest for the present study. First we shall consider the point source and line sink individually, and then we shall combine them to form a closed dividing streamline.

A.1 POINT SOURCE

The dividing streamline for a point source in a uniform flow (P. 457, Ref. 2) is given by:

$$\frac{r}{R_m} = \frac{1}{2} \csc \frac{\phi}{2} \tag{A.1}$$

where, as indicated in the Sketch A.1,

$$R = r \sin \phi, \quad x = r \cos \phi, \quad \pi R_m^2 V = Q$$

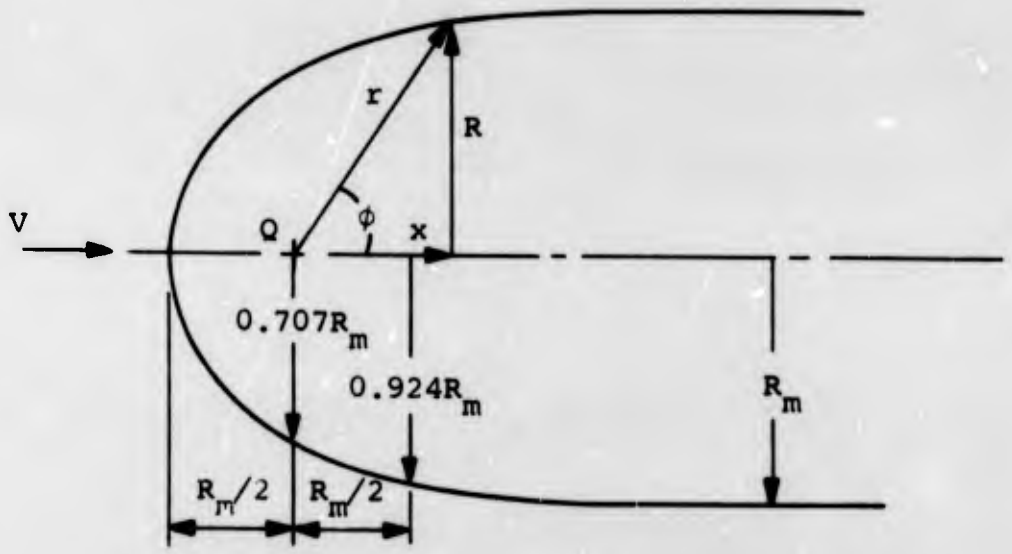

Sketch A.1.- Dividing streamline for point source and uniform flow.

A.2 LINE SINK

The dividing streamline for a line sink of uniform strength Q and length a (p. 458, Ref. 2) can be shown to be given by:

$$\frac{x}{a} = \frac{1}{2} \pm \sqrt{\frac{1}{4} - f}$$

where

$$f = \frac{R^2}{R_m^2}\left(1 - \frac{R^2}{R_m^2}\right) - \frac{R_m^2}{4a^2}\,\frac{\left(1 - \frac{2R^2}{R_m^2}\right)^2}{1 - \frac{R^2}{R_m^2}} \qquad (A.2)$$

$$-Qa = \pi R_m^2 V$$

and where the $\pm$ sign is for

$$R \gtrless \sqrt{\frac{1}{2}}\, R_m \quad \text{or} \quad x \gtrless \frac{a}{2}$$

The nomenclature and shape of the dividing streamline are shown in Sketch A.2 for $R_m = 0.175a$

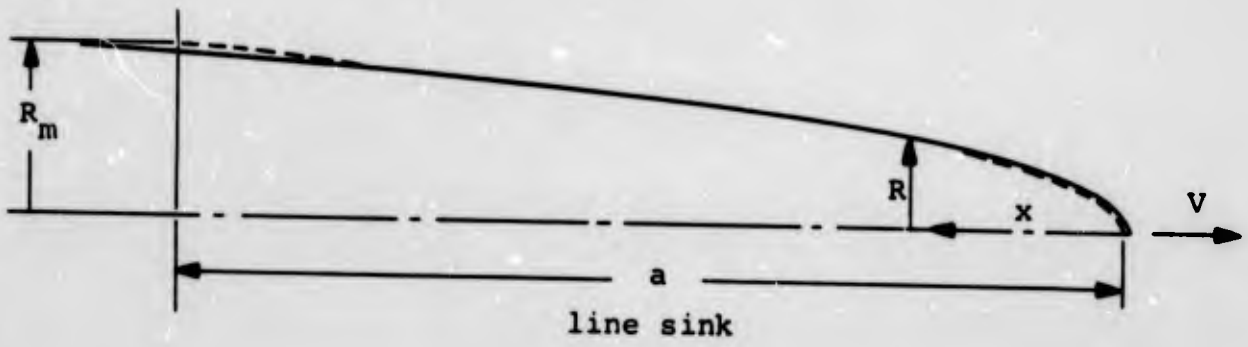

Sketch A.2.- Dividing streamline for a line sink and free stream.

At the leading edge of the sink the dividing streamline has approached the asymptote. That is, at $x = a$,

$$\frac{R^2}{R_m^2} \simeq 1 - \frac{R_m}{8a} \quad \text{if} \quad R_m \ll a \qquad (A.3)$$

Over the line sink the dividing streamline can be approximated by the parabola associated with slender-body theory, that is, if $0 < x < a$

$$\frac{R^2}{R_m^2} = 1 - \frac{x}{a} \tag{A.4}$$

as shown dashed in the foregoing sketch for comparison.

A.3 POINT SOURCE LINE SINK

It is evident from the preceding results that, if the point source link are combined to form a closed dividing streamline or hull shape, then the shapes of the hull nose and boattail are given approximately by Equations (A.1) and (A.2), independently. The accuracy of this approximation will be illustrated for the extreme case when the point source is put at the leading edge of the line sink. In this case it can be shown (with the use of Ref. 2) that the dividing streamline is given exactly by the parametric expressions

$$\frac{R^2}{R_m^2} = -\left(\frac{R_m}{a}\right)^2 \frac{a^2}{4r^2} - \frac{r}{a} + \sqrt{1 + \frac{a}{r}\left(\frac{R_m}{a^2}\right)^2}$$

$$\frac{x}{r} = -\left(\frac{R_m}{a}\right)^2 \frac{a^2}{2r^2} + \sqrt{1 + \frac{a}{r}\left(\frac{R_m}{a}\right)^2} \tag{A.5}$$

The streamline is plotted to scale in Sketch A.3 for $R_m/a = 0.141$.

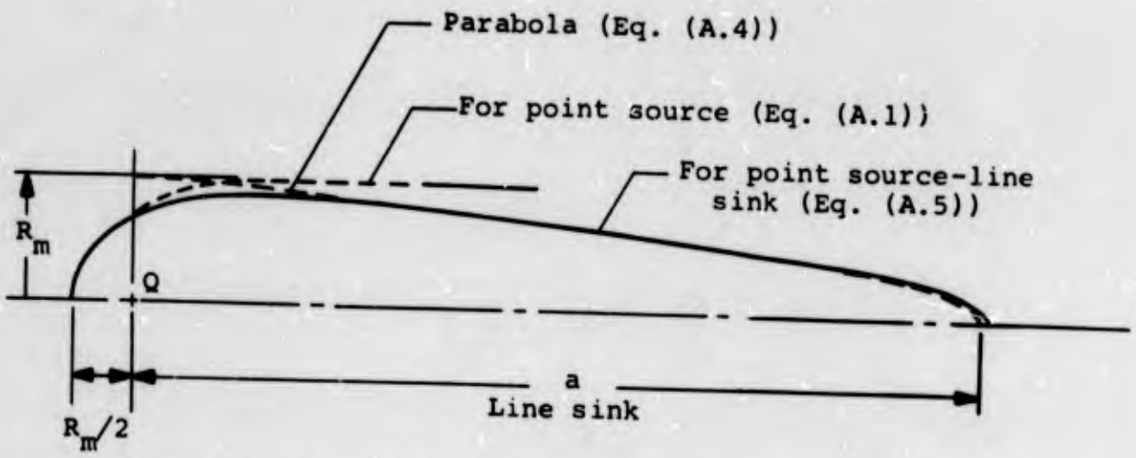

Sketch A.3.- Dividing streamline for a point source line sink in uniform flow.

Equations (A.1) and (A.4) are also shown for comparison. Thus, it is evident that, for reasonably slender hull shapes corresponding to a combined point source line sink in a uniform flow:

(1) The entire dividing streamline can be estimated accurately by fairing the curves given by Equations (A.1) and (A.2) for the individual source and sink.

(2) Furthermore, the shape of the boattail is nearly parabolic as given by Equation (A.4).

By trial and error, the gap between the point source and line sink can be chosen such that the dividing streamline approximates the shape of typical torpedo and submarine hulls, as shown in Figure 2, where the dashed hull shapes were found by fairing Equations (A.1) and (A.2) for the individual point source and line sink. For the submarine hull of interest (Fig. 2(b)), the simple parabola, Equation (A.4), compares well with Equation (A.2) near the aft end of the hull as shown in Figure 3.

APPENDIX B

EFFECT OF THE DUCTED PROPELLER ON THE HULL BOUNDARY CONDITION

Here we shall estimate the effect of the ducted propeller on the hull boundary condition. We shall do this by computing the velocity induced by the ducted propeller at a finite number of points on the hull boattail. We shall then add an equal number of point sources to the line sink which represents the boattail, and require that the sinks cancel the velocity induced through the boattail surface by the ducted propeller. Finally, the incremental forces caused by the addition of the point sources will be determined.

B.1 INDUCED VELOCITY

To compute the velocity components induced by the ducted propeller at the boattail surface, we shall approximate the boattail with the parabola (Eq. (3)) and we shall concentrate the duct-bound vorticity into a ring vortex at the duct leading edge as indicated in Sketch B.1.

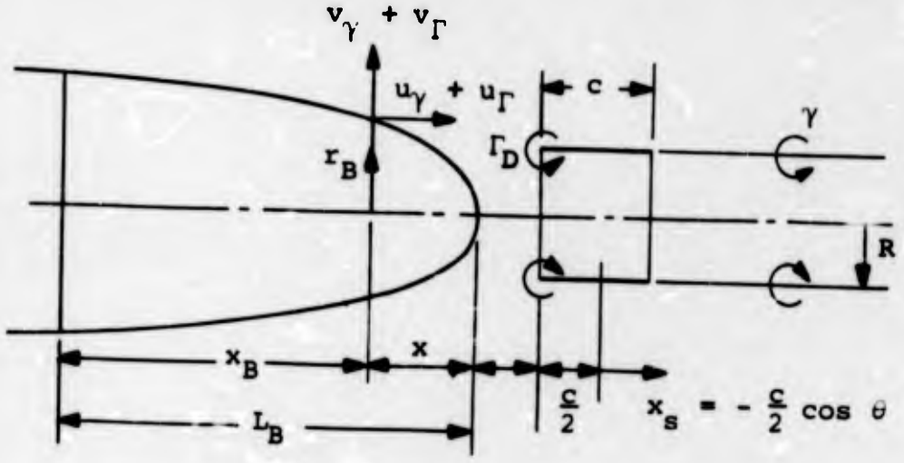

Sketch B.1.- Nomenclature for induced velocity.

The vortex cylinder shed by the actuator disk extends along the duct downstream from its leading edge and contributes to the duct circulation by the amount γc.[1] The remainder of the duct circulation is given by

[1]The disk is assumed to be at the duct inlet here as in Section 3.

$$\Gamma_D = \int_{-c/2}^{+c/2} \gamma_D \, dx_s \tag{B.1}$$

Substitution of Equation (16) for γ_D and integration gives

$$\Gamma_D = \frac{\pi}{2} c\gamma \left(C_o + \frac{C_1}{2} \right) \tag{B.2}$$

where the Fourier coefficients C_o and C_1 are given by Equations (40) with $R_n = 0$ for a cylindrical duct.

The radial velocity component induced by the vortex cylinder is given by Equation (A.5) of Reference 3 as

$$v_\gamma = \frac{\gamma R}{\pi \sqrt{r_B'}} \left(\frac{E - K}{k_\gamma} + \frac{k_\gamma K}{2} \right) \tag{B.3}$$

where the argument for K and E is

$$k_\gamma^2 = \frac{4r_B'}{(1 + r_B')^2 + (S' + x')^2}$$

and the nomenclature is shown in Sketch B.1. From Equation (3)

$$r_B' = R_m' \sqrt{\frac{x'}{L_B'}} \tag{B.4}$$

The prime denotes division by R.

The radial velocity component induced by the vortex ring is given by Equation (64) of Reference 3 or Equation (27), page 307 of Reference 9, as

$$v_\Gamma = - \frac{\Gamma_D}{2\pi D} \frac{k_\Gamma x'}{(r_B')^{3/2}} \left(K - \frac{1 - \frac{k_\Gamma^2}{2}}{1 - k_\Gamma^2} E \right) \tag{B.5}$$

where $k_\gamma = k_\Gamma$.

For the axial velocity components (u_γ, u_Γ) induced by the vortex ring and vortex cylinder, the computed values listed in Tables 15 and 16 of Reference 8 will be used.[2]

For the assumed configuration corresponding to Case 4-1 in Table IV we have

$$R_m' = 2.63, \quad L_B' = 15, \quad S' = -\frac{1}{2}, \quad c' = 1$$

$$\frac{\gamma}{V} = 0.244, \quad C_o = 1.436, \quad C_1 = -0.810, \quad \Gamma_D = 1.620\, c\gamma$$

The induced velocity components computed by the foregoing procedure at the points indicated in Table V are listed in the first three columns of that table. The choice of the number and location of these points is arbitrary; however, it can be seen in Table V that the induced velocity is small beyond one duct diameter upstream of the duct (where $x_n' > 2.5$). In Table V, we have defined $u_{DP} \equiv u_\gamma + u_\Gamma$, and u_p is the part of u_γ which is induced by the portion of the vortex cylinder downstream of the duct.

B.2 POINT SOURCES

We shall use three different arrangements of point sources equally spaced along the centerline as indicated in Table V. The velocity components induced by the n^{th} source at the i^{th} point on the hull boattail are

$$u'_{q_{i,n}} = \frac{(R_m')^2\, q_n'(x_n' - x_i')}{4\left[(x_n' - x_i')^2 + (r_i')^2\right]^{3/2}}$$

$$v'_{q_{i,n}} = \frac{(R_m')^2\, q_n' r_i'}{4\left[(x_n' - x_i')^2 + (r_i')^2\right]^{3/2}} \qquad \text{(B.6)}$$

where the prime denotes division of the velocities by V and division of the source strengths by $Q = \pi R_m^2 V$.

To satisfy the hull boundary condition at the boattail and at the same axial stations as the point sources, we have at the i^{th} point along the hull surface

---

[2] An analytical expression for u_γ has subsequently become available (Ref. 9).

$$v'_{DP_i} + v'_{q_i} = -\left(\frac{dr_B}{dx}\right)_i \left(u'_{DP_i} + u'_{q_i}\right) \tag{B.7}$$

where the slope of the hull surface is, from Equation (B.4),

$$\left(\frac{dr_B}{dx}\right)_i = \frac{R_m}{2L'_B\left(r'_B\right)_i} \tag{B.8}$$

and the velocity components induced by the point sources are, from Equation (B.6),

$$u'_{q_i} = \frac{(R'_m)^2}{4} \sum^{n} \frac{q'_n(x'_n - x'_i)}{\left[(x'_n - x'_i)^2 + \left(r'_B\right)^2_i\right]^{3/2}}$$

$$v'_{q_i} = \frac{(R'_m)^2}{4} \sum^{n} \frac{q'_n r'_i}{\left[(x'_n - x'_i)^2 + \left(r'_B\right)^2_i\right]^{3/2}} \tag{B.9}$$

Substitution of Equations (B.8) and (B.9) and the values of u'_{DP_i}, v'_{DP_i} from Table V into Equation (B.7) gives a set of equations for the strengths of the sources q'_n. Solution of the equations by machine gives the source strengths given in Table V for the three sets of points chosen for Cases 4-1-A, B, C. It is evident that the distribution of strength for each set of points is ragged and the distribution varies drastically between the three sets. The net forces due to the three sets of point sources are more consistent, however, as will be shown next.

B.3 INCREMENTAL HULL DRAG

The incremental hull drag force caused by the addition of the point sources are

$$\Delta D_H = -\rho \sum q_n u_n \tag{B.10}$$

or in coefficient form

$$\Delta C'_H \equiv \frac{\Delta D_H}{A_m q} = -2 \sum q'_n u'_n$$

where u_n is the axial velocity at the n^{th} source due to the free stream, hull wake, duct, and propeller. Except for computational error the sum of the source strengths must equal zero for the dividing streamline representing the hull to be closed at both ends. The computed sum is small for each of the three cases, as shown in Table V. The corresponding incremental hull drag coefficient due to the free stream is, from Equation (B.10)

$$\Delta C'_{H(V)} = -2 \sum q'_n = \begin{array}{l} -0.0026 \text{ for Case 4-1-A} \\ -\ .0026 \text{ for Case 4-1-B} \\ -\ .0036 \text{ for Case 4-1-C} \end{array}$$

Since this incremental drag is zero except for computational error, it will be neglected. The incremental drag due to the hull wake will be neglected because of the initial assumption that this drag is independent of the presence of the ducted propeller. The incremental hull drag caused by the ducted propeller is caused by the axial velocity u_{DP} induced along the centerline by the vortex cylinder and vortex ring. Using Equation (26), page 306 of Reference 8, and Equation (C.2) we find

$$u_{DP} = u_\gamma + u_\Gamma = \frac{\gamma}{2}\left(1 - \frac{x' + S'}{\sqrt{(x' + S')^2 + 1}}\right) + \frac{\Gamma_D}{D} \frac{1}{\left[(x' + S')^2 + 1\right]^{3/2}} \tag{B.11}$$

Substitution of Equation (B.11) into (B.10) gives the incremental hull drag coefficient from the ducted propeller acting upon the point sources as

$$\Delta C'_{H(DP)} = -2 \sum q'_n \left(u'_{DP}\right)_n \tag{B.12}$$

The incremental drag due to the duct $\Delta C'_{H(D)}$ cancels with the duct thrust generated by the point sources. Hence $\Delta C'_{H(P)}$ gives the incremental change in the net force on the hull-duct configuration cuased by the addition of the point sources. This force is generated by the "free" portion of the vortex cylinder which extends from the duct trailing edge. Thus we find that

$$\Delta C'_{H(P)} = -2 \sum q'_n \left(u'_P\right)_n \tag{B.13}$$

where

$$\left(u'_P\right)_n = \frac{\gamma}{2V}\left[1 - \frac{x'_n + S' + c'}{\sqrt{(x'_n + S' + c')^2 + 1}}\right]$$

Equations (B.12) and (B.13) are evaluated in Table V. It can be seen that the hull interference from the ducted propeller $C'_{H(DP)}$ and from the duct $C'_{H(D)}$ increase about 17 percent because of the addition of the point sources for all three computational cases. However, the net force on the hull-duct configuration C'_P changes by $\Delta C'_{H(P)}$ which is less than a 3.5 percent change for all three cases. Thus, the flow induced by the ducted propeller through the hull appears to have little effect upon the forces except for the hull-duct interaction which is independent of the other forces.

APPENDIX C

EFFECT OF THE DUCTED PROPELLER ON HULL DRAG

Here we shall determine the induced hull drag (or thrust deduction) caused by interference with the ducted propeller. As described in Section 2.2 the hull drag caused by the duct-bound vorticity is equal to the duct thrust caused by hull interference, and the latter is found directly from the present solution. The remainder of the interference is the hull drag, caused by the vorticity trailing from the duct. This drag is generated by the axial velocity induced along the point source line sink which represents the hull in the first iteration. That is,

$$D_{H(P)} = \rho \int_{\xi_1}^{\xi_2} u_\gamma \frac{Q}{L_B} d\xi - \rho Q \left(u_\gamma\right)_Q \qquad (C.1)$$

with the nomenclature of Sketch C.1.

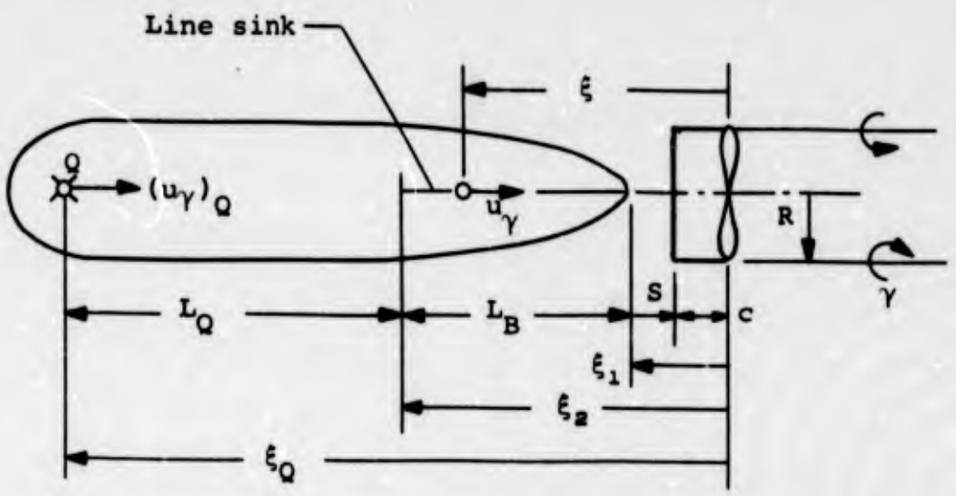

Sketch C.1.- Nomenclature for hull drag.

The axial velocity induced by the vortex cylinder γ along the centerline can be found by integration of the velocity induced by each elementary vortex ring of the cylinder. This gives

$$u_\gamma = \frac{\gamma}{2}\left(1 - \frac{\xi'}{\sqrt{(\xi')^2 + 1}}\right) \tag{C.2}$$

where $\xi' = \xi/R$.

Substitution into Equation (C.1) gives

$$D_{H(P)} = \frac{\rho Q \gamma}{2L'_B} \int_{S'+c'}^{S'+c'+L'_B} \left(1 - \frac{\xi'}{\sqrt{\xi'^2 + 1}}\right) d\xi' - \rho Q \frac{\gamma}{2}\left(1 - \frac{\xi'_Q}{\sqrt{\xi'^2_Q + 1}}\right) \tag{C.3}$$

The first terms in the parentheses cancel, and substitution of Equation (4) for Q gives

$$D_{H(P)} = \pi R_m^2 \frac{\rho V^2}{2} \frac{\gamma}{V}\left[\frac{\xi'_Q}{\sqrt{(\xi'_Q)^2 + 1}} - \frac{1}{L'_B}\int_{S'+c'}^{S'+c'+L'_B} \frac{\xi'\, d\xi'}{\sqrt{(\xi')^2 + 1}}\right] \tag{C.4}$$

Integration gives the hull drag coefficient due to propeller interference as

$$C'_{H(P)} = \frac{D_{H(P)}}{Aq} = \frac{\gamma}{V}\left\{\frac{\xi'_Q}{\sqrt{(\xi'_Q)^2 + 1}} + \frac{1}{L'_B}\left[\sqrt{(S' + c')^2 + 1} - \sqrt{(S' + c' + L_B)^2 + 1}\right]\right\}$$

$$\equiv \frac{\gamma}{V} Y \tag{C.5}$$

where $\xi'_Q = c' + S' + L'_B + L'_Q$.

When $S' + c' \ll 1$ we can use the approximation

$$C'_{H(P)} = \frac{\gamma}{V}\left[\frac{L'_B + L'_Q}{\sqrt{\left(L'_B + L'_Q\right)^2 + 1}} + \frac{1 - \sqrt{\left(L'_B\right)^2 + 1}}{L'_B}\right] \tag{C.6}$$

For the assumed hull shape we have (Eq. (1))

$$\frac{L_B}{R_m} = 5.72, \quad \frac{L_Q}{R_m} = 7.65$$

Hence, for the assumed values $S' + c' = 0$, $R'^2_m = 2$, we have $L'_B = 11.44$, $L'_Q = 15.30$ and from Equation (C.6)

$$C'_{H(P)} = 0.091 \frac{\gamma}{V}$$

Thus, the hull drag coefficient due to the vorticity trailing from the duct $C'_{H(P)}$ is not negligibly small compared with the isolated hull drag coefficient, $C'_H = 0.050$, unless the propeller is very lightly loaded such that $\gamma \ll V$.

BLANK PAGE

APPENDIX D

EFFECT OF DUCT PROFILE THICKNESS

Here we shall examine the assumption that the effect of duct profile thickness is negligibly small for the present analysis. The profile thickness can be represented by a distribution of elementary ring sources along the duct chord $q_D(x_s)$ as shown in Reference 7. First we shall estimate the net force on the entire configuration caused by the addition of the ring source distribution. This force is generated by the two components of free vorticity, that is, the slipstream and hull wake vortex cylinders acting upon the ring sources q_D along the duct chord. The interaction forces between q_L and the vorticity bound to the hull and duct cancel and do not contribute to the net force on the configuration. Since the duct profile is closed, the total strength of the ring source distribution must be zero; that is,

$$\int_{-c/2}^{+c/2} q_D(x_s)\, dx_s = 0 \tag{D.1}$$

The duct thrust caused by the addition of thickness is

$$T_{D_t} = +\rho\pi D \int_{-c/2}^{c/2} (V + u) q_D\, dx_s \tag{D.2}$$

where u is the axial velocity component induced along the duct chordline by the free vortex cylinders comprising the wake and slipstream, or γ_W and γ. It is evident that T_{D_t} is caused by only the <u>variation</u> of u along the duct chord. To estimate T_{D_t} we shall assume that the duct thickness distribution corresponds to that for a point source Q at the leading edge of a constant line sink. Furthermore, we shall fit a parabola to three computed values of u at the leading and trailing edges and midchord of the duct as indicated below.

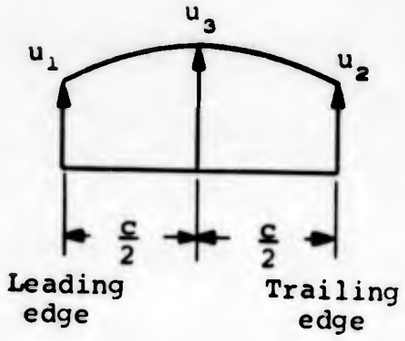

We then find from Equation (D.2) that

$$C_{D_t} = \frac{T_{D_t}}{Aq} = \frac{4t_h}{3R}\left(\frac{5u_1 - u_2 - 4u_3}{V}\right) \tag{D.3}$$

where the duct thickness at midchord is

$$t_h = \frac{Q}{2V} \tag{D.4}$$

For the part of C_{D_t} caused by the vortex cylinder γ trailing from the duct, evaluation of $u_{1,2,3}$ from Table 15 of Reference 8, gives

$$\left(C_{D_t}\right)_\gamma = -0.590\,\frac{t_h}{c}\,\frac{\gamma}{V} \tag{D.5}$$

The part of C_{D_t} caused by the vortex cylinders in the hull wake can also be estimated by use of Table 15 of Reference 8 to evaluate $u_{1,2,3}$. For the geometric configuration of Case 4 in Table IV and for one, two, or three vortex cylinders representing the hull wake as in Figure 4, we find the following values:

Number of wake cylinders, z	C_p	$\frac{\gamma}{V}$	$\frac{u_1}{V}$	$\frac{u_2}{V}$	$\frac{u_3}{V}$	$\frac{3c}{4t_h}\left(C_{D_t}\right)_{\gamma_W}$ (Eq. (D.3))
1	0.379	0.244	0.045	0.022	0.035	0.063
2	.379	.222	.015	.010	.014	.031
3	.380	.217	-.088	-.091	-.087	.017

Let us take the geometric configuration of Case 4-2 with two wake cylinders and add duct thickness such that $t_h = (1/10)c$. We find from the foregoing table and Equation (D.5) that

$$\left(C_{D_t}\right)_{\gamma_W} + \left(C_{D_t}\right)_{\gamma} = 0.004 - 0.013 = -0.009$$

Hence, from the initial discussion of this appendix, it can be seen that the drag force on the entire configuration increases by an amount 0.009 Aq because of the addition of duct thickness. To put the configuration back in force equilibrium, we should increase the thrust coefficient of the ducted propeller by the amount 0.009. However, this is a negligible increase (2 percent) since the thrust coefficients of the duct and propeller are 0.379 and 0.45, respectively.

BLANK PAGE

INITIAL DISTRIBUTION LIST
(PART I)

Chief of Naval Research
Department of the Navy
Washington 25, D. C.
Attn: Codes 438 (3)

Commanding Officer
Office of Naval Research Branch Office
495 Summer Street
Boston 10, Massachusetts (1)

Commanding Officer
Office of Naval Research Branch Office
219 S. Dearborn Street
Chicago 1, Illinois (1)

Commanding Officer
Office of Naval Research Branch Office
207 West 24th Street
New York 11, New York (1)

Commanding Officer
Office of Naval Research Branch Office
Navy 100, Box 39, Fleet Post Office
New York, New York (25)

Commanding Officer
Office of Naval Research Branch Office
1030 East Green Street
Pasadena 1, California (1)

Commanding Officer
Office of Naval Research Branch Office
1000 Geary Street
San Francisco 9, California (1)

Director
Naval Research Laboratory
Washington 25, D. C.
Attn: Codes 2000 (1)
2020 (1)
2027 (6)

Chief, Bureau of Ships
Department of the Navy
Washington 25, D. C.
Attn: Codes 300 (1)
305 (1)
210L (3)
341B (1)
342A (1)
345 (1)
420 (1)
421 (1)
440 (1)
442 (1)
525 (1)
634A (1)

Chief, Bureau of Naval Weapons
Department of the Navy
Washington 24, D. C.
Attn: Codes R (1)
R-12 (1)
RAAD (1)
RR (1)
RRRE (1)
RU (1)
RUTO (1)

Director, Special Projects Office
Department of the Navy
Washington 25, D. C.
Attn: Codes SP-001 (1)
SP-201 (1)

Chief, Bureau of Yards and Docks
Department of the Navy
Washington 25, D. C.
Attn: Codes D-202 (1)
D-400 (1)
E-500 (1)

Commanding Officer and Director
David Taylor Model Basin
Washington 7, D. C.
Attn: Code 513 (75)

Commander
U. S. Naval Ordnance Laboratory
Silver Spring, Maryland
Attn: Dr. A. May (1)
Desk DA (1)
Desk DR (1)
Desk HL (1)

Commander
U. S. Naval Ordnance Test Station
China Lake, California
Attn: Mr. J. W. Hicks (1)
Codes 753 (1)
4032 (1)
5014 (1)

Commander
U. S. Naval Ordnance Test Station
Pasadena Annex
3202 E. Foothill Blvd.
Pasadena 8, California
Attn: Mr. J. W. Hoyt (1)
Research Division (1)
P508 (1)
P804 (1)
P807 (1)
P80962 (Library Section) (1)

Superintendent
U. S. Naval Academy
Annapolis, Maryland
Attn: Library (1)

Commanding Officer and Director
U. S. Naval Engineering
Experiment Station
Annapolis, Maryland
Attn: Code 750 (1)

Superintendent
U. S. Naval Postgraduate School
Monterey, California
Attn: Library (1)

Commanding Officer and Director
U. S. Naval Electronic Laboratory
San Diego 52, California
Attn: Code 4223 (1)

Commander
Norfolk Naval Shipyard
Portsmouth, Virginia (1)

Commander
New York Naval Shipyard
Naval Base
Brooklyn 1, New York (1)

Commander
Boston Naval Shipyard
Boston 29, Massachusetts (1)

Commander
Philadelphia Naval Shipyard
Naval Base
Philadelphia 12, Pennsylvania (1)

Commander
Portsmouth Naval Shipyard
Portsmouth, New Hampshire
Attn: Design Division (1)

Commander
Charleston Naval Shipyard
U. S. Naval Base
Charleston, South Carolina (1)

Commander
Puget Sound Naval Shipyard
Bremerton, Washington (1)

Commander
Long Beach Naval Shipyard
Long Beach 2, California (1)

Commander
Pearl Harbor Naval Shipyard
Navy #128, Fleet Post Office
San Francisco, California (1)

Commanding Officer
NROTC and Naval Administrative Unit
Massachusetts Institute of
Technology
Cambridge 39, Massachusetts (1)

Commanding Officer
U. S. Naval Underwater Ordnance
Station
Newport, Rhode Island
Attn: Research Division (1)

Commanding Officer and Director
U.S. Navy Mine Defense Laboratory
Panama City, Florida (1)

Commander
San Francisco Naval Shipyard
San Francisco 24, California (1)

Commander
Mare Island Naval Shipyard
Vallejo, California (1)

Air Force Office of Scientific
Research
Mechanics Division
Washington 25, D. C. (1)

Defense Documentation Center
Cameron Station
Alexandria, Virginia (20)

Office of Technical Services
Department of Commerce
Washington 25, D. C. (1)

Fluid Mechanics Section
National Bureau of Standards
Washington 25, D. C.
Attn: Dr. G. B. Schubauer (1)

Director
Engineering Science Division
National Science Foundation
Washington, D. C. (1)

National Academy of Sciences
National Research Council
2101 Constitution Ave., N.W.
Washington 25, D. C. (1)

The Johns Hopkins University
Baltimore 18, Maryland
Attn: Professor S. Corrsin (1)
Professor F. H. Clauser (1)
Professor O. M. Phillips (1)

Director
Applied Physics Laboratory
The John Hopkins University
8621 Georgia Avenue
Silver Spring, Maryland (1)

California Institute of Technology
Pasadena 4, California
Attn: Hydrodynamics Laboratory (1)
Professor T. Y. Wu (1)
Professor A. T. Ellis (1)
Professor A. J. Acosta (1)
Professor M. S. Plesset (1)
Dr. J. Laufer (1)

University of California
Berkeley 4, California
Attn: Department of Engineering (1)
Professor H. A. Schade (1)
Professor J. W. Johnson (1)
Professor J. V. Wehausen (1)

Director
Scripps Institution of Oceanography
University of California
La Jolla, California (1)

Iowa Institute of Hydraulic Research
State University of Iowa
Iowa City, Iowa
Attn: Professor H. Rouse (1)
Professor L. Landweber (1)
Professor P. G. Hubbard (1)

Harvard University
Cambridge 38, Massachusetts
Attn: Professor G. Birkhoff (1)
Professor G. F. Carrier (1)
Professor S. Goldstein (1)
Professor B. Budiansky (1)

University of Michigan
Ann Arbor, Michigan
Attn: Engineering Research Inst. (1)
Professor R. B. Couch

Webb Institute of Naval Architecture
Glen Cove, Long Island, New York
Attn: Professor E. V. Lewis (1)
Technical Library (1)

Institute of Mathematical Sciences
New York University
25 Waverly Place
New York 3, New York
Attn: Professor J. J. Stoker (1)
Professor A. Peters (1)
Professor J. Keller (1)
Professor R. Courant (1)

Director
Ordnance Research Laboratory
Pennsylvania State University
University Park, Pennsylvania
Attn: Dr. E. J. Skudrzyk (1)
Dr. G. F. Wislicenus (1)
Dr. M. Sevik (1)

Director
St. Anthony Falls Hydraulic
Laboratory
Minneapolis 14, Minnesota
Attn: Mr. J. N. Wetzel (1)
Professor B. Silberman (1)
Professor E. R. Eckert (1)

Massachusetts Institute of Technology
Cambridge 39, Massachusetts
Attn: Professor P. Mandel (1)
Professor M. Abkowitz (1)
Dr. Leon H. Schindel (1)

Stevens Institute of Technology
Davidson Laboratory
Hoboken, New Jersey
Attn: Mr. D. Savitsky (1)
Mr. J. P. Breslin (1)
Dr. S. J. Lukasik (1)
Mr. H. W. MacDonald (1)
Mr. E. Numata (1)
Dr. P. N. Hu (1)

Dr. L. L. Higgins
Space Technology Laboratories Inc.
Canoga Park Facility
8433 Fallbrook Avenue
Canoga Park, California (1)

Dr. A. Ritter
Therm Advanced Research Division
Therm, Inc.
Ithaca, New York (1)

Hydronautics, Incorporated
Pindell School Road
Howard County
Laurel, Maryland
Attn: Mr. P. Eisenberg, Pres. (1)
Mr. M. P. Tulin, Vice Pres. (1)

Technical Research Group, Inc.
Route 110
Melville, Long Island, New York
Attn: Dr. J. Kotick (1)

AiResearch Manufacturing Company
9851-9951 Sepulveda Boulevard
Los Angeles 45, California
Attn: Blaine R. Parking (1)

Hydrodynamics Laboratory
Convair
San Diego 12, California
Attn: Mr. H. E. Brooke (1)
Mr. R. H. Oversmith (1)

Aerojet-General Corporation
6352 N. Irwindale Avenue
Azusa, California
Attn: Mr. C. A. Gongwer (1)

Republic Aviation Corporation
Farmingdale, Long Island, New York
Attn: Mr. J. Malloy, Manager
Hydrospace Systems Div. (1)

Department of Engineering Mechanics
University of Notre Dame
Notre Dame, Indiana
Attn: Professor A. G. Strandhagen (1)

Stanford University
Stanford, California
Attn: Dr. Bryne Perry (1)

Aeronautical Engineering Department
Catholic University of America
Washington, D. C.
Attn: Professor M. Munk, Head (1)

Department of Aeronautical
Engineering
University of Colorado
Boulder, Colorado
Attn: Professor M. S. Uberoi (1)

ASW and Ocean Systems Department
Lockheed Aircraft Corporation
Burbank, California
Attn: Mr. G. W. Paper (1)

Electric Boat Division
General Dynamics Corporation
Groton, Connecticut
Attn: Mr. R. McCandliss (1)

Missile Development Division
North American Aviation, Inc.
Downey, California
Attn: Dr. E. R. Van Driest (1)

U. S. Rubber Company
Research and Development Department
Wayne, New Jersey
Attn: Mr. L. M. White (1)

Douglas Aircraft Company, Inc.
Aircraft Division
Long Beach, California
Attn: Mr. A. M. O. Smith (1)

Unclassified
Security Classification

DOCUMENT CONTROL DATA · R&D
(Security classification of title, body of abstract and indexing annotation must be entered when the overall report is classified)

1. ORIGINATING ACTIVITY *(Corporate author)*
Vidya Division, Itek Corporation

2a. REPORT SECURITY CLASSIFICATION
Unclassified

2b. GROUP

3. REPORT TITLE
Interference Between a Hull and a Stern-Mounted Ducted Propeller

4. DESCRIPTIVE NOTES *(Type of report and inclusive dates)*
Technical Report, Oct. 1, 1963 to Oct. 1, 1964

5. AUTHOR(S) *(Last name, first name, initial)*
Kriebel, Anthony R.

6. REPORT DATE	7a. TOTAL NO. OF PAGES	7b. NO. OF REFS
Sept. 30, 1964	34 plus Appendixes	10

8a. CONTRACT OR GRANT NO.	9a. ORIGINATOR'S REPORT NUMBER(S)
Nonr 4278(00)	161
b. PROJECT NO. 9066	
c. Task 1	9b. OTHER REPORT NO(S) *(Any other numbers that may be assigned this report)*
d.	

10. AVAILABILITY/LIMITATION NOTICES

11. SUPPLEMENTARY NOTES	12. SPONSORING MILITARY ACTIVITY
Theoretical Analysis of Hydrodynamic Interference for an Axisymmetric Underwater Hull	See Cover

13. ABSTRACT

The hydrodynamic interference between an underwater hull and a stern-mounted ducted propeller is predicted by theoretical analysis. The analysis assumes axially symmetric potential flow, and the hull wake vorticity is concentrated into multiple vortex cylinders extending downstream from the boattail. The interference forces are predicted versus the following geometric parameters with the hull shape held fixed to represent TMB Model 4620: duct chord-to-diameter ratio, duct size, duct axial spacing from hull, axial location of propeller within duct, duct camberline shape, and number of vortex cylinders used to represent hull wake. Also, the effect of duct profile thickness upon the analytical results is estimated and shown to be small.

The computed results show that cylindrical ducts are unsuitable for propulsion of the assumed hull shape because, at cruising speed, they are ineffective in reducing the propeller thrust, they have large leading-edge suction, and they produce large hull interference. However, when duct camber is added, the results also show that if all of the other geometric parameters are specified, a duct camberline can be designed so that the duct carries more thrust than the propeller without any leading-edge suction or hull interference.

DD FORM 1 JAN 64 1473

Unclassified
Security Classification

14. KEY WORDS	LINK A		LINK B		LINK C	
	ROLE	WT	ROLE	WT	ROLE	WT
Theory Hydrodynamics Interference Hull Ducted Propeller Propeller						

INSTRUCTIONS

1. ORIGINATING ACTIVITY: Enter the name and address of the contractor, subcontractor, grantee, Department of Defense activity or other organization *(corporate author)* issuing the report.

2a. REPORT SECURITY CLASSIFICATION: Enter the overall security classification of the report. Indicate whether "Restricted Data" is included. Marking is to be in accordance with appropriate security regulations.

2b. GROUP: Automatic downgrading is specified in DoD Directive 5200.10 and Armed Forces Industrial Manual. Enter the group number. Also, when applicable, show that optional markings have been used for Group 3 and Group 4 as authorized.

3. REPORT TITLE: Enter the complete report title in all capital letters. Titles in all cases should be unclassified. If a meaningful title cannot be selected without classification, show title classification in all capitals in parenthesis immediately following the title.

4. DESCRIPTIVE NOTES: If appropriate, enter the type of report, e.g., interim, progress, summary, annual, or final. Give the inclusive dates when a specific reporting period is covered.

5. AUTHOR(S): Enter the name(s) of author(s) as shown on or in the report. Enter last name, first name, middle initial. If military, show rank and branch of service. The name of the principal author is an absolute minimum requirement.

6. REPORT DATE: Enter the date of the report as day, month, year; or month, year. If more than one date appears on the report, use date of publication.

7a. TOTAL NUMBER OF PAGES: The total page count should follow normal pagination procedures, i.e., enter the number of pages containing information.

7b. NUMBER OF REFERENCES: Enter the total number of references cited in the report.

8a. CONTRACT OR GRANT NUMBER: If appropriate, enter the applicable number of the contract or grant under which the report was written.

8b, 8c, & 8d. PROJECT NUMBER: Enter the appropriate military department identification, such as project number, subproject number, system numbers, task number, etc.

9a. ORIGINATOR'S REPORT NUMBER(S): Enter the official report number by which the document will be identified and controlled by the originating activity. This number must be unique to this report.

9b. OTHER REPORT NUMBER(S): If the report has been assigned any other report numbers *(either by the originator or by the sponsor)*, also enter this number(s).

10. AVAILABILITY/LIMITATION NOTICES: Enter any limitations on further dissemination of the report, other than those imposed by security classification, using standard statements such as:

(1) "Qualified requesters may obtain copies of this report from DDC."

(2) "Foreign announcement and dissemination of this report by DDC is not authorized."

(3) "U. S. Government agencies may obtain copies of this report directly from DDC. Other qualified DDC users shall request through _____."

(4) "U. S. military agencies may obtain copies of this report directly from DDC. Other qualified users shall request through _____."

(5) "All distribution of this report is controlled. Qualified DDC users shall request through _____."

If the report has been furnished to the Office of Technical Services, Department of Commerce, for sale to the public, indicate this fact and enter the price, if known.

11. SUPPLEMENTARY NOTES: Use for additional explanatory notes.

12. SPONSORING MILITARY ACTIVITY: Enter the name of the departmental project office or laboratory sponsoring *(paying for)* the research and development. Include address.

13. ABSTRACT: Enter an abstract giving a brief and factual summary of the document indicative of the report, even though it may also appear elsewhere in the body of the technical report. If additional space is required, a continuation sheet shall be attached.

It is highly desirable that the abstract of classified reports be unclassified. Each paragraph of the abstract shall end with an indication of the military security classification of the information in the paragraph, represented as *(TS), (S), (C), or (U)*.

There is no limitation on the length of the abstract. However, the suggested length is from 150 to 225 words.

14. KEY WORDS: Key words are technically meaningful terms or short phrases that characterize a report and may be used as index entries for cataloging the report. Key words must be selected so that no security classification is required. Identifiers, such as equipment model designation, trade name, military project code name, geographic location, may be used as key words but will be followed by an indication of technical context. The assignment of links, roles, and weights is optional.

Vidya Division, Itek Corporation
1450 Page Mill Road, Palo Alto, California
INTERFERENCE BETWEEN A HULL AND A STERN-MOUNTED DUCTED PROPELLER,
by Anthony R. Kriebel
Vidya Report No. 161, September 1964, 71 pages, 8 illus.,
(Contract No. Nonr-4278(00)) Unclassified report

The hydrodynamic interference between an underwater hull and a stern-mounted ducted propeller is predicted by theoretical analysis. The analysis assumes axially symmetric potential flow, and the hull wake vorticity is concentrated into multiple vortex cylinders extending downstream from the boattail. The interference forces are predicted versus the following geometric parameters with the hull shape held fixed to represent TMB Model 4620: duct chord-to-diameter ratio, duct size, duct axial spacing from hull, axial location of propeller within duct, duct camberline shape, and number of vortex cylinders used to represent hull wake. Also, the effect of duct profile thickness upon the analytical results is estimated and shown to be small.

The computed results show that cylindrical ducts are unsuitable for propulsion of the assumed hull shape because, at cruising speed, they are ineffective in reducing the propeller thrust, they have large leading-edge suction, and they produce large hull interference. However, when duct camber is added, the results also show that if all of the other geometric parameters are specified, a duct camberline can be designed so that the duct carries more thrust than the propeller without any leading-edge suction or hull interference.

UNCLASSIFIED

1. Interference, hull-ducted propeller
2. Ducted propeller
3. Propulsion, underwater

I Kriebel, A. R.

Vidya Division, Itek Corporation
1450 Page Mill Road, Palo Alto, California
INTERFERENCE BETWEEN A HULL AND A STERN-MOUNTED DUCTED PROPELLER,
by Anthony R. Kriebel
Vidya Report No. 161, September 1964, 71 pages, 8 illus.,
(Contract No. Nonr-4278(00)) Unclassified report

The hydrodynamic interference between an underwater hull and a stern-mounted ducted propeller is predicted by theoretical analysis. The analysis assumes axially symmetric potential flow, and the hull wake vorticity is concentrated into multiple vortex cylinders extending downstream from the boattail. The interference forces are predicted versus the following geometric parameters with the hull shape held fixed to represent TMB Model 4620: duct chord-to-diameter ratio, duct size, duct axial spacing from hull, axial location of propeller within duct, duct camberline shape, and number of vortex cylinders used to represent hull wake. Also, the effect of duct profile thickness upon the analytical results is estimated and shown to be small.

The computed results show that cylindrical ducts are unsuitable for propulsion of the assumed hull shape because, at cruising speed, they are ineffective in reducing the propeller thrust, they have large leading-edge suction, and they produce large hull interference. However, when duct camber is added, the results also show that if all of the other geometric parameters are specified, a duct camberline can be designed so that the duct carries more thrust than the propeller without any leading-edge suction or hull interference.

UNCLASSIFIED

1. Interference, hull-ducted propeller
2. Ducted propeller
3. Propulsion, underwater

I Kriebel, A. R.

Vidya Division, Itek Corporation
1450 Page Mill Road, Palo Alto, California
INTERFERENCE BETWEEN A HULL AND A STERN-MOUNTED DUCTED PROPELLER,
by Anthony R. Kriebel
Vidya Report No. 161, September 1964, 71 pages, 8 illus.,
(Contract No. Nonr-4278(00)) Unclassified report

The hydrodynamic interference between an underwater hull and a stern-mounted ducted propeller is predicted by theoretical analysis. The analysis assumes axially symmetric potential flow, and the hull wake vorticity is concentrated into multiple vortex cylinders extending downstream from the boattail. The interference forces are predicted versus the following geometric parameters with the hull shape held fixed to represent TMB Model 4620: duct chord-to-diameter ratio, duct size, duct axial spacing from hull, axial location of propeller within duct, duct camberline shape, and number of vortex cylinders used to represent hull wake. Also, the effect of duct profile thickness upon the analytical results is estimated and shown to be small.

The computed results show that cylindrical ducts are unsuitable for propulsion of the assumed hull shape because, at cruising speed, they are ineffective in reducing the propeller thrust, they have large leading-edge suction, and they produce large hull interference. However, when duct camber is added, the results also show that if all of the other geometric parameters are specified, a duct camberline can be designed so that the duct carries more thrust than the propeller without any leading-edge suction or hull interference.

UNCLASSIFIED

1. Interference, hull-ducted propeller
2. Ducted propeller
3. Propulsion, underwater

I Kriebel, A. R.

Vidya Division, Itek Corporation
1450 Page Mill Road, Palo Alto, California
INTERFERENCE BETWEEN A HULL AND A STERN-MOUNTED DUCTED PROPELLER,
by Anthony R. Kriebel
Vidya Report No. 161, September 1964, 71 pages, 8 illus.,
(Contract No. Nonr-4278(00)) Unclassified report

The hydrodynamic interference between an underwater hull and a stern-mounted ducted propeller is predicted by theoretical analysis. The analysis assumes axially symmetric potential flow, and the hull wake vorticity is concentrated into multiple vortex cylinders extending downstream from the boattail. The interference forces are predicted versus the following geometric parameters with the hull shape held fixed to represent TMB Model 4620: duct chord-to-diameter ratio, duct size, duct axial spacing from hull, axial location of propeller within duct, duct camberline shape, and number of vortex cylinders used to represent hull wake. Also, the effect of duct profile thickness upon the analytical results is estimated and shown to be small.

The computed results show that cylindrical ducts are unsuitable for propulsion of the assumed hull shape because, at cruising speed, they are ineffective in reducing the propeller thrust, they have large leading-edge suction, and they produce large hull interference. However, when duct camber is added, the results also show that if all of the other geometric parameters are specified, a duct camberline can be designed so that the duct carries more thrust than the propeller without any leading-edge suction or hull interference.

UNCLASSIFIED

1. Interference, hull-ducted propeller
2. Ducted propeller
3. Propulsion, underwater

I Kriebel, A. R.